NAVAL POSTGRADUATE SCHOOL
Monterey, California

THESIS

NANOMECHANICS MODEL
FOR STATIC EQUILIBRIUM

by

Sunghoon Jung

September 2002

Thesis Advisor: Young W. Kwon

Approved for public release; distribution is unlimited

THIS PAGE INTENTIONALLY LEFT BLANK

REPORT DOCUMENTATION PAGE			Form Approved OMB No. 0704-0188
Public reporting burden for this collection of information is estimated to average 1 hour per response, including the time for reviewing instruction, searching existing data sources, gathering and maintaining the data needed, and completing and reviewing the collection of information. Send comments regarding this burden estimate or any other aspect of this collection of information, including suggestions for reducing this burden, to Washington headquarters Services, Directorate for Information Operations and Reports, 1215 Jefferson Davis Highway, Suite 1204, Arlington, VA 22202-4302, and to the Office of Management and Budget, Paperwork Reduction Project (0704-0188) Washington DC 20503.			
1. AGENCY USE ONLY *(Leave blank)*	**2. REPORT DATE** September 2002	**3. REPORT TYPE AND DATES COVERED** Master's Thesis	
4. TITLE AND SUBTITLE: Nanomechanics Model for Static Equilibrium			**5. FUNDING NUMBERS**
6. AUTHOR(S) **Sunghoon Jung**			
7. PERFORMING ORGANIZATION NAME(S) AND ADDRESS(ES) Naval Postgraduate School Monterey, CA 93943-5000			**8. PERFORMING ORGANIZATION REPORT NUMBER**
9. SPONSORING /MONITORING AGENCY NAME(S) AND ADDRESS(ES) N/A			**10. SPONSORING/MONITORING AGENCY REPORT NUMBER**
11. SUPPLEMENTARY NOTES The views expressed in this thesis are those of the author and do not reflect the official policy or position of the Department of Defense or the U.S. Government.			
12a. DISTRIBUTION / AVAILABILITY STATEMENT Approved for public release; distribution is unlimited			**12b. DISTRIBUTION CODE**

13. ABSTRACT ***(maximum 200 words)***

This study presented a computational technique to model and simulate atomistic behavior of materials under static loads. Interatomic potential energy was used to maintain equilibrium among atoms under static loads and constraints. In addition, the atomistic model was coupled with the finite element analysis model so that more flexible loads and constraints could be applied to the atomistic model. A multi-scale technique was also presented for some single wall nanotubes of both zigzag and armchair and then their effective stiffness were estimated. Those designed nanotubes are woven into fabric composites, which can be used in various military applications including body armors, armored vehicles, and infantry transportation vehicles because advanced nano-composites could be much lighter and stronger than current ones. Some example problems were presented to illustrate the developed technique for the nano-composites and SWNTs. The proposed technique for nanomechanics can be used for design and analysis of materials at the atomic or molecular level.

14. SUBJECT TERMS Nanomechanics, nanocomposite, atomistic model, molecular dynamics, finite element analysis, static equilibrium, multi-scale technique.			**15. NUMBER OF PAGES** 73
			16. PRICE CODE
17. SECURITY CLASSIFICATION OF REPORT Unclassified	**18. SECURITY CLASSIFICATION OF THIS PAGE** Unclassified	**19. SECURITY CLASSIFICATION OF ABSTRACT** Unclassified	**20. LIMITATION OF ABSTRACT** UL

NSN 7540-01-280-5500 Standard Form 298 (Rev. 2-89)
Prescribed by ANSI Std. 239-18

THIS PAGE INTENTIONALLY LEFT BLANK

Approved for public release; distribution is unlimited

NANOMECHANICS MODEL FOR STATIC EQUILIBRIUM

Sunghoon Jung
Captain, Republic of Korea Army
B.S. In Physics, Korea Military Academy, 1997

Submitted in partial fulfillment of the
requirements for the degree of

MASTER OF SCIENCE IN MECHANICAL ENGINEERING

from the

NAVAL POSTGRADUATE SCHOOL
September 2002

Author: Captain Sunghoon Jung

Approved by: Young W. Kwon
Thesis Advisor

Young W. Kwon
Chairman, Department of Mechanical Engineering

THIS PAGE INTENTIONALLY LEFT BLANK

ABSTRACT

This study presented a computational technique to model and simulate atomistic behavior of materials under static loads. Interatomic potential energy was used to maintain equilibrium among atoms under static loads and constraints. In addition, the atomistic model was coupled with the finite element analysis model so that more flexible loads and constraints could be applied to the atomistic model. A multi-scale technique was also presented for some single wall nanotubes of both zigzag and armchair and then their effective stiffness were estimated. Those designed nanotubes are woven into fabric composites, which can be used in various military applications including body armors, armored vehicles, and infantry transportation vehicles because advanced nano-composites could be much lighter and stronger than current ones. Some example problems were presented to illustrate the developed technique for the nano-composites and SWNTs. The proposed technique for nanomechanics can be used for design and analysis of materials at the atomic or molecular level.

THIS PAGE INTENTIONALLY LEFT BLANK

TABLE OF CONTENTS

THIS PAGE INTENTIONALLY LEFT BLANK

LIST OF FIGURES

THIS PAGE INTENTIONALLY LEFT BLANK

ACKNOWLEDGMENTS

First of all, I feel really thankful to my country for giving me chance to study here in an outstanding and beautiful place.

Also, the author wishes to give his appreciation to his thesis advisor, Professor Young W. Kwon, for his guidance and assistance. His passionate guidance was critical in the completion of this research.

Lastly, my most sincere appreciation is owed to my loving parents and sister, as well as my friends in my homeland. Their confident support and trust for me was always in my heart and led me to the completion of successful research in Monterey, CA.

THIS PAGE INTENTIONALLY LEFT BLANK

EXECUTIVE SUMMARY

There have been a lot of efforts to perform the nanoscale simulation, which is based on the potential function among the atoms. The first simulation technique was the classical molecular dynamics model. These days, with more quantum mechanics calculation, more accurate simulation techniques are developed such as TBMD, Carparrinello MD method, and ab initio method.

In this study, a nanoscale computational technique was developed for atomic or molecular equilibrium under static loads. The technique was based on interactive force equilibrium among atoms from varous potential functions of classical MD method. The interaction among atoms was described by nonlinear springs among them with internal forces. The nanoscale atomic model was coupled with the finite element method so that boundary conditions could be applied more readily to the model. Some sample examples that are comparable to the continuum mechanics were simulated and quite reasonable results were obtained.

Then, two types of single wall carbon nanotubes, either in armchair or zigzag pattern, were designed to estimate their effective stiffness, which is quite close to the experimental value. Furthermore, the modulus of the nanotube increased slightly with the diameter of SWNT.

Based on the estimated elastic modulus of SWNT, the developed computational technique was implemented into a multi-scale analysis of a composite structure that can be highly applicable in military. Some examples were given for woven fabric composites hypothetically made of carbon nanotubes.

The results of numerical examples were discussed and compared with other studies and experimental data qualitatively. The developed nanoscale computational technique was computationally efficient and would be a useful tool for design and analysis of materials at the atomic or molecular level.

THIS PAGE INTENTIONALLY LEFT BLANK

I. INTRODUCTION

A. BACKGROUND

These days, a lot of researchers have been contributing their efforts to perform the nanoscale simulation to see how the mechanics in nanoscale works or if their nanodesign can be modeled practically or not. For their simulations, they have to find the force field function, describing the real world as close as possible, among atoms. Actually, finding the same force field function as real world is the hardest part in this research field. Recently, the quantum mechanics, which deals with the mechanics in very small scale such as electron, quark, etc., has been used to derive the force field function. It seems like that the force field is getting close to the one of real world by using the quantum mechanics. By virtue of the quantum mechanics, some simulation technique, such as tight binding method, ab inition method, Carparrinello MD method, has been developed.

In this section, those simulation techniques: TBMD, ab inition, classical method, which are recently important and frequently used, are introduced. In addition, mechanical properties of nanotubes and carbon nanotube composite materials from recent researchers are examined, which is associated with the investigation of Young's modulus of SWNT and CNT composite materials in this thesis.

1. Computational Techniques for Nanoscale Simulations

In 1960's, some analytical methods are used to compute an infinite system such as thermodynamic properties of interacting, bulk condensed-matter systems. But these analytical methods had some drawbacks, for those were just valid in a weakly interacting system limit and the approximations still had to be carried out numerically beyond a few orders. From that time, a tremendous effort was performed into finding a new kind of approximation scheme. An exact numerical computation of the properties of a finite-sample system has become the most common approach to studying interacting condensed-matter systems. Molecular dynamics (MD) is commonly used technique in which the motion of atoms can be treated in an approximate finite difference equation of Newtonian. The MD has been exploited widely besides dealing with very light atoms and very low temperatures.

When MD began to be used, MD computations mainly used simple pair potentials to describe simple phase systems such as inert gases in condensed-phase systems, and the materials with hexagonal closed packing structures [1]. As time went by, more complex systems were needed to be described such as metals and semiconductors with explicit or implicit many-body force-field functions. It began with embedded-atom-method type potentials for metals and bond-order type potentials for semiconductors. Researchers thought most cases would be solved based on the variations of these three types of potentials. However, there was no universal classical potential that provides successful results for all materials in all scenarios. So, more attention to the description of dynamics with surfaces and clusters were needed. [1]

For years, quantum MD schemes have been used to compute forces among atoms at each time step with quantum mechanics calculations within the Born-Oppenheimer approximation and the results were quite accurate [4]. But still the dynamic motions for atomic positions are calculated by Newtonian or Hamiltonian mechanics and described by MD. The most widely known and accurate scheme is the Carparrinello MD method, which describes the electronic states and atomic forces within the local density approximation using the ab initio density functional method. Ab initio MD simulations now are just performed for the systems, which are composed of a few hundred atoms [4]. With large size scale of system, such calculation begins to expand their computational resources. In the perspective of system size, the intermediate technique between large-scale classical MD and small-scale quantum Carparrinello MD methods are semi empirical quantum simulation approaches that cover an important range of system size where classical potentials are not accurate enough and ab initio computations are not feasible. The tight-binding molecular dynamics approach thus provides an important bridge between the accurate ab initio quantum MD and classical MD methods [4].

Therefore, in computational techniques for nanoscale simulation, those three simulations: tight-binding molecular dynamics (TBDM), ab initio quantum MD, and classical MD method, can be used in a complementary manner to improve computational accuracy and efficiency. We can first investigate an atomic structure of nanosystem. Then, we can examine its mechanical or electronic behavior through static ab initio

electronic energy minimization schemes or through studies of the system's quantum conductance behavior. When two nanoscale systems are brought together or taken apart, we can get highly accurate information on mechanical or electronic behavior from using the ab initio method [1,2].

Subsequently, the three important simulation methods mentioned previously, will be examined in following sections. In reference, the most important method in this paper is the classical molecular method that is used for this paper's MATLAB program.

a. Tight-Binding Molecular Dynamics (TBMD)

Commonly, it is said that the atom is composed of a set of quantum mechanical particles, nuclei, and electrons, and they are formulated by the schroedinger equation below [1],

$$H\phi[\{R_I, r_i\}] = E_{tot}\phi[\{R_I, r_i\}] \tag{1}$$

in which the full quantum many-body Hamiltonian operator is

$$H = \sum \frac{P_I^2}{2M_I} + \sum \frac{Z_I Z_J e^2}{R_{IJ}} + \sum \frac{p_i^2}{2m_e} + \sum \frac{e^2}{r_{ij}} - \sum \frac{Z_I e^2}{|R_I - r_i|} \tag{2}$$

where R_I and r_i are nuclei and electron coordinates. Applying the Born-Oppenheimer approximation, we can assumes that the electronic degrees of freedom follow adiabatically the corresponding nuclear positions, and the nuclei coordinates become classical variables. This assumption reduces the full quantum many-body problem of equation (1) to the quantum many-electron problem as below [1],

$$H[R_I]\psi[r_i] = E_{el}\psi[r_i] \tag{3}$$

where

$$H = \sum \frac{P_I^2}{2M_I} + H(\{R_I\}) \tag{4}$$

Correspondingly, the Hamiltonian operator, equation (2) is reduced as shown in equation (4). In the tight-binding method, an approximation can make the quantum many-electron problems much simpler. We assume that the crystal potential is

strong enough for the electron to remain at the site for a while when an ion holds an electron during its motion through the lattice. While the ion is holding the electrons, it is thought that other atoms around a single ion usually do not affect the electron orbits so that its state function corresponds to that of an atomic orbital because the electrons are tightly bounded to its own atom [1].

One of the advantages of the tight-binding method is to find an energy-minimized structure of a nanoscale system without considering symmetry constraints [4]. From time to time, a symmetry-unconstrained dynamic energy minimization of a system helps us find the system's global energetic minimum, which is not easily interpreted on the symmetry consideration by itself. The parallelization of the tight-binding method code means that we need to parallelize the direct diagonalization part as well as the MD part [1]. Usually, it is hard to parallelize a sparse symmetric matrix with many eigenvalues and eigenvectors and that is a cumbersome part in the simulation of large intermediate-range system.

b. Ab initio Simulation Method.

The complex quantum many-body Schroedinger equations with numerical algorithm have to be introduced to explain the ab initio or first principles method, which means that ab initio method is one of the quantum mechanics simulation methods. The tight-binding method described previously is another quantum mechanics simulation method based on the linear combination of atomic orbital approximations to describe the quantum mechanical electronic wave functions. Due to the simple basis expansion using atomic orbitals, the tight binding method is approximately 1000 times more efficient than the ab initio method. But, the ab initio method gives us a more accurate description of quantum mechanics behavior of materials properties even though it restricts system size to several hundreds atoms. So, these three simulation methods (MD, TBMD, ab initio) compose a complementary set of simulation tools to investigate a variety of atomic-scale processes in nanodevice modeling.

The ab initio method has been developed from significant mathematical contributions. One of them is to verify a theorem that the ground state energy of a many-electron system is a function of total electron density, $\rho(r)$, rather than the full electron

wave function, $\varphi[r_i]: E_{el}(\varphi[r_i]) \equiv E_{el}(\rho(r))$. The Hamiltonian operator H and schroedinger equation are given by [1]

$$H[R_I] = \sum \frac{P_I^2}{2M_I} + \sum \frac{Z_I Z_J e^2}{R_{IJ}} + \sum \frac{p_i^2}{2m_e} + \sum \frac{e^2}{r_{ij}} - \sum \frac{Z_I e^2}{|R_I - r_i|} \tag{5}$$

and

$$H[R_I]\psi[r_i] = E_{el}\psi[r_i] \tag{6}$$

where $\{R_I\}$ and $\{r_i\}$ are atomic positions and electronic coordinates. The density functional theory is derived from the fact that the ground state total electronic energy is a functional of the system's electron density.

Furthermore, the theory of Walter Kohn and Lu Sham makes things much simpler. They have shown that the density functional theory can be reformulated as a single-electron problem with self-consistent effective potential including all the exchange-correlation effects of electronic interactions [1]:

$$H_1 = \frac{p^2}{2m_e} + V_H(r) + V_{XC}[\rho(r)] + V_{ion-el}(r), \tag{7}$$

$$H_1\psi_i(r) = \varepsilon_i\psi(r), i = 1, ..., N_{tot}, \tag{8}$$

$$\rho(r) = \sum |\varphi_i(r)|^2 \tag{9}$$

This single-electron Schroedinger equation (9) called the Kohn-Sham equation (the local density approximation) approximates the unknown effective exchange-correlation potential. This combined method has successfully predicted materials properties without using any experimental inputs other than the identity of the constituent atoms. With widely used packages for density functional theory simulation, the ab initio simulation method is a major computational materials research tool.

c. Classical MD Method.

In Classical MD, atoms or molecules move into the equilibrium position as many of the atoms and molecules in the vicinity are interacting one other. Basically the

forces between atoms or molecules can be derived from the Hamilton's classical equation of motion from Newton's second law below [1]:

$$F_I = \frac{d^2 R_I}{dt^2} = -\frac{dV}{dR_I} \tag{10}$$

$$H = \sum \frac{P_I^2}{2M_I} + V(\{R_I\}) \tag{11}$$

$$F_I(\{R_I\}) = -\frac{dV}{dR_I}, \tag{12}$$

which is used to construct Hamilton's classical equations of motion, which are second-order ordinary differential equations.

Every atom or molecule moves and acts like a particle that is moving in the many-body force fields of other similar particles. The atomic and molecular interactions describing the dynamics are thus given by classical many-body force-field functions, and we can write the atomic interaction energy function $V(\{R_I\})$ in terms of pair and many-body interactions that depend on relative distances among different atoms. The atomic forces are analytic derivatives of the interaction energy functions as shown in the last equation above.

After these equations are approximated as finite-difference equations with discrete time step Δt, the standard Gear's fifth-order predictor-corrector may be used to solve them. The simulations can be performed under a variety of thermodynamic equilibrium or nonequilibrium conditions, and we can describe reactions between atoms and molecules as the molecular building blocks approach depending on the force-field function used [4].

In this thesis, the Tersoff-Brenner many-body potential has been used to describe atomic interactions in carbon-based systems such as carbon nanotubes. One of very outstanding aspects of the Tersoff-Brenner potential is that short-range bonded interactions are reactive so that chemical bonds can form and break during simulation. With the well-defined potential energy function, the MD code is applied to a collection of

atoms. Then the equations of motion are numerically integrated forward in finite time steps by using a predictor-corrector method. When it comes to the cost, the computational cost of the many-body bonded interactions is relatively high compared to the cost of similar methods with no reactive interactions that have simpler functional forms.

2. Nanomechanics of Carbon Nanotubes.

a. Carbon Nanotube

As shown in Figure 1 below, the carbon nanotubes is a fullerene-related structure, which is composed of a graphene cylinder and closed with end caps containing pentagonal rings. It was discovered in 1991 by the electron microscopist Sumio Iijima who was studying the material deposited on the cathode during the arc-evaporation synthesis of fullerenes. He found that the central core of the cathodic deposit contained a variety of closed graphitic structures including nanoparticles and nanotubes, which had never been observed previously. After finding those structures, Thomas Ebbesen and Pulickel Ajayan, from Iijima's lab, showed how nanotubes could be produced in bulk quantities by varying the arc-evaporation conditions. This opened a revolutional way to the experiment for various properties of carbon nanotubes all over the world.

So, the carbon arc evaporation method became the first way to fabricate the carbon nanotubes. Recently, some other ways have been found to produce the nanotubes, which are laser ablation or pulsed laser vaporization method, chemical vapor deposition method and recently high-pressure CO conversion method for bulk of SWNT.

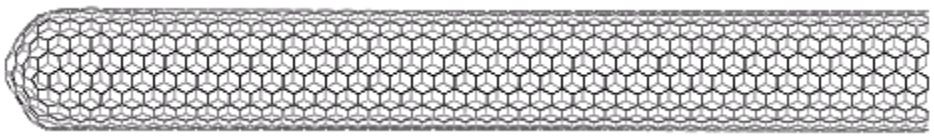

(a) SWNT

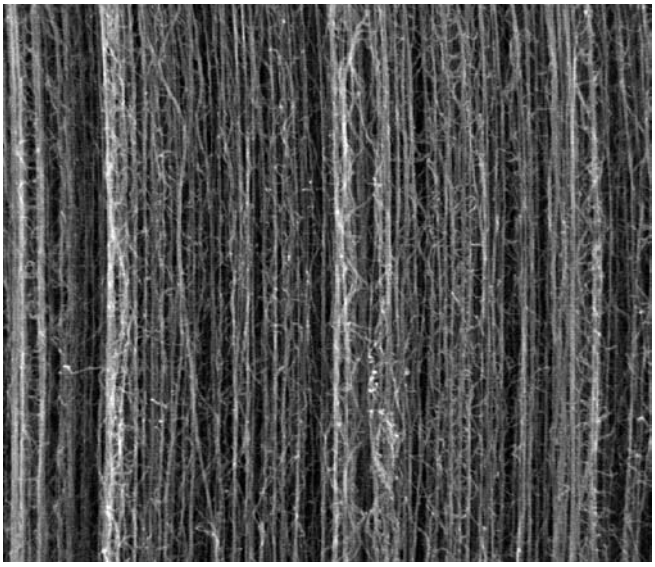

(b) Side view of a bundle of carbon nanotube from SEM

Figure 1. Nanotube

b. Mechanical Properties of Carbon Nanotube

After the nanotube was found, further investigation has shown that Single Wall Carbon Nanotubes (SWNT) and Multi Wall Carbon Nanotubes (MWNT) have outstandingly strong and stiff mechanical characteristics along the axis of nanotube and flexible characteristics along the normal to the tube's axis. The Young's modulus of a SWNT is expressed as $Y = \partial^2 E / V \partial \varepsilon^2$, where E is the strain energy and V is the volume of the nanotube. When some simulation techniques mentioned before are used, the Young's modulus of nanotube approximately ranged from 1 to 1.2 Tpa which are mostly within the range of experimental observations. It is interesting that SWNT has stiffer than MWNT for the axial strain because it has smaller radii of curvature and relatively defect free structure. But for non-axial strain, the MWNT is much stiffer [2].

The bending stiffness of a SWNT is expressed as $d^2 E / LdC^2$, in which E is the total strain energy, L is the length, and C is the curvature of the bent nanotube. From the simulation, the bending Young's modulus of SWNT varied with diameter; the bending modulus decreases with the increase in tube diameter. For a small diameter SWNT the bending modulus was about 0.9 Tpa. In torsional stiffness, which is described as $K = d^2 E / Ld\theta^2$, where E is the total strain energy and θ is the torsion angle, there is a

relation between the torsion stiffness and the shear modulus. From some simulation, the shear modulus of a carbon nanotube was found to be 0.3 Tpa and it was not remarkably dependent of the tube diameter [2].

In the perspective of compression using classical molecular dynamics simulations with Tersoff-Brenner potential, it is shown that the tubes are extremely stiff under axial compression, and the system remains within elastic limit even for very large deformations like 15% strain [5,6].

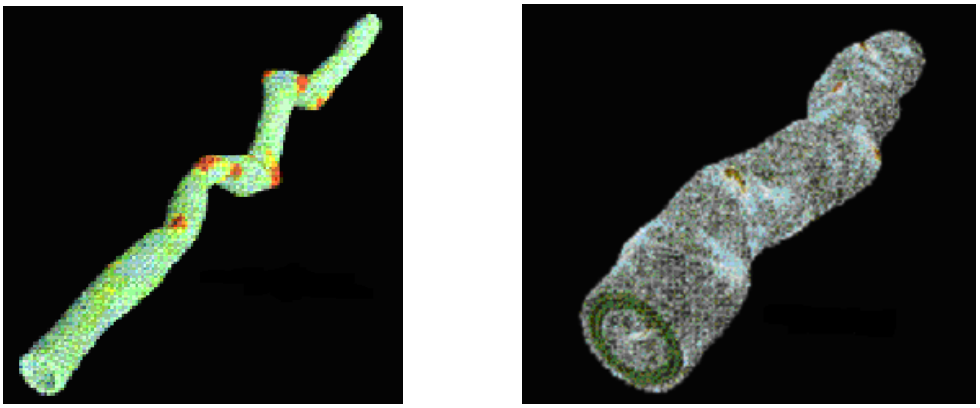

(a) (b)

Figure 2. Axial compression and plastic collapse of (a) SWNT, (b) MWNT [2]

When the SWNTs and MWNTs are compressed beyond elastic limits, they undergo a sideway buckling, which is associated with nonlinear elastic instability, as shown in Figure 2 [2]. But once the external load disappears, the system returns to the original state. Deformations such as plastic collapses or fractures of thin nanotubes without any buckling also appear in experiments, but these deformations have never appeared in classical MD simulations with the Tersoff-Brenner potential.

c. Mechanical Properties of CNT Composite Materials

Since the nanotube has very good electrical and thermal conduction capabilities, it can be recommended for composite materials with light weight and multi-function. But simulations of nanotube-polymer composites are so far not widely performed. It is expected for the resulting composite materials to have the outstanding mechanical, thermal and electrical characteristics of individual SWNTs and MWNTs in a

polymer, ceramic or metal matrix. There were some efforts to investigate characteristics of nanotube-polymer composite materials. From most measurements, it was suggested that there was a very modest increase in strength properties of CNT-polymer matrices compared to original polymer matrices. Also there were a few attempts to characterize mechanical and thermal properties of CNT composite materials with MD simulations. In preliminary MD investigations of the nanotube-polymer composites above glass transition temperature, the thermal expansion coefficient of the composite matrix and diffusion coefficients of the polymer molecules increase significantly over their bare polymer matrix values [2]. Mixing 5-10% of nanotubes in the polyethylene polymers increases the thermal expansion coefficient by as much as 40%[3].

A SWNT is usually a hard material possessing a Poisson ratio of 0.1 to 0.1 while polyethylene is a softer polymeric material with Poisson ration of about 0.44. Due to the difference of the Poisson ratio, there is a resistance from the hard fibers to their surrounding matrix and the tensile stress causes the compressive pressure in the composite materials when the composite containing SWNT is under tensile strain. Thus, from that mechanism, the modulus of a composite can be enhanced even when bonding between the SWNT fibers and the polymer matrix is not very good. So the Young's moduli of the nanotube-polymer composites are found to be increased by about 30% for strain [7].

B. OBJECTIVES

Recently, much attention has been devoted to the study of material behavior at the atomic or molecular level. For example, there has been extensive research in carbon nanotubes [8-10] because they have very high stiffness and strength. Other nanoscale researches focused on the crack behavior and fracture [12-17].

Those studies used molecular dynamics models or atomic models to simulate the material behavior at the nano-scale [18,19]. Most of the simulations were dynamic analysis using Newton's second law and different potential energies among neighboring atoms or molecules. Static equilibrium positions are time averages of the dynamic equilibrium motions. It is quite a time consuming process to compute the static equilibrium positions of atoms or molecules from dynamic analysis.

In this study, there are some efforts to develop a computational technique to model and simulate atomic behavior under static loads and constraints. In addition, in order to make it easy to apply various loads and constraints, the atomic model was coupled with finite element model. The atomic model is a discrete model while the finite element model is a continuum model. Furthermore, some SWNTs with varying diameter are modeled to predict the elastic modulus of those SWNTs by using developed computational technique and compare the results to other studies and experimental data. Finally, the modulus of nanotube composite is to be examined for two different types of woven fabric composites as well.

THIS PAGE INTENTIONALLY LEFT BLANK

II. ATOMIC MODEL

A. ATOMIC FORCE POTENTIAL ENERGY

The atomic model is based on equilibrium of interatomic forces along with boundary conditions. The interatomic forces are computed from the potential energy. There are many potential energies proposed so far depending on the nature of material and their chemical bonds. One of the commonly used potential energies for metals has been the Morse function while the Abell-Tersoff-Brenner potential has been adopted for carbon, hydrogen, and hydrocarbons.

The Morse function describes the potential energy $\Phi(r_{ij})$ of two atoms *i* and *j* with a distance r_{ij} as below

$$\Phi(r_{ij}) = D\left[e^{-2\alpha(r_{ij}-r_o)} - 2e^{-\alpha(r_{ij}-r_o)}\right] \tag{1}$$

in which *D* and α are constants with dimensions of energy and reciprocal distance, respectively. The r_o is the equilibrium distance of the two atoms with $\Phi(r_o) = -D$ as shown in Equation (1). The constants in Equation (1) were provided in Reference [15] for various pure metals. The force between the two atoms is computed from

$$\vec{F}(r_{ij}) = -\frac{\partial \Phi}{\partial r_{ij}}\vec{n}_r \tag{2}$$

in which $\vec{n}_r$ is the unit position vector between the two atoms. The forces among *N* atoms in a given system must be in equilibrium using Equation (2).

The Abell-Tersoff-Brenner potential for carbon is expressed as

$$\Phi(r_{ij}) = V_R(r_{ij}) - \overline{B}_{ij} V_A(r_{ij}) \tag{3}$$

where

$$V_R(r_{ij}) = f_{ij}(r_{ij}) D_{ij}^{(e)} / (S_{ij} - 1) e^{-\sqrt{2S_{ij}}\beta_{ij}(r_{ij} - R_{ij}^{(e)})} \tag{4}$$

$$V_A(r_{ij}) = f_{ij}(r_{ij}) D_{ij}^{(e)} S_{ij} / (S_{ij} - 1) e^{-\sqrt{2/S_{ij}}\beta_{ij}(r_{ij} - R_{ij}^{(e)})} \tag{5}$$

$$f_{ij} = \begin{cases} 1 & r_{ij} \le R_{ij}^{(1)} \\ \left[1+\cos\left(\dfrac{\pi(r_{ij}-R_{ij}^{(1)})}{R_{ij}^{(2)}-R_{ij}^{(1)}}\right)\right]/2 & R_{ij}^{(1)} < r_{ij} < R_{ij}^{(2)} \\ 0 & r_{ij} \ge R_{ij}^{(2)} \end{cases} \quad (6)$$

$$\overline{B}_{ij} = (B_{ij} + B_{ji})/2 + F_{ij}(N_i^{(t)}, N_j^{(t)}, N_{ij}^{conj}) \quad (7)$$

$$B_{ij} = \left[1 + \sum_{k(\neq i,j)} G_i(\theta_{ijk}) f_{ik}(r_{ik}) e^{\alpha_{ijk}\left\{(r_{ij}-R_{ij}^{(e)})-(r_{ij}-R_{ij}^{(e)})\right\}} + H_{ij}(N_i^{(H)}, N_i^{(C)})\right]^{-\delta_i} \quad (8)$$

$$G(\theta) = a_o\left[1 + \frac{c_o^2}{d_o^2} - \frac{c_o^2}{\left\{d_o^2 + (1+\cos\theta)^2\right\}}\right] \quad (9)$$

Here, θ is the angle between atoms *i-j* and *i-k*. The constant values in these equations are provided for carbon, hydrogen, and hydrocarbons in Reference [16].

B. ATOMIC FORCE EQUILIBRIUM

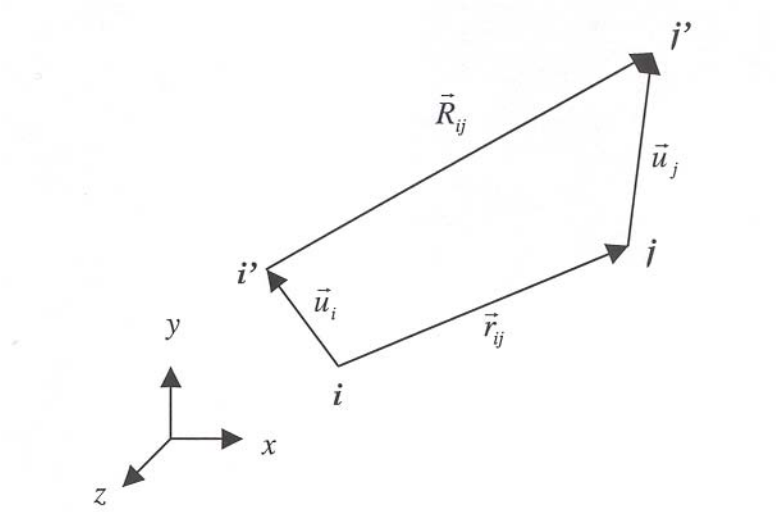

Figure 3. Relative positions of two atoms before and after movement

Consider any two atoms that are located at *i* and *j* as shown in Figure 3. The present position vector from atom *i* to *j* is denoted by $\vec{r}_{ij}$. Let each atom be displaced by $\vec{u}_i$ and $\vec{u}_j$, respectively, to the new positions *i*' and *j*'. Then, the new position vector between the two atoms is expressed as $\vec{R}_{ij}$. The displacement vectors and position vectors are related as

$$\vec{R}_{ij} = \vec{r}_{ij} + \vec{u}_j - \vec{u}_i = \vec{r}_{ij} + \Delta\vec{u}_{ij} \tag{10}$$

where $\Delta\vec{u}_{ij} = \vec{u}_j - \vec{u}_i$ is the relative displacement vector of the two atoms.

The force between atoms *i* and *j* at the new positions is expressed as Equation (4),

$$\vec{F}_{ij}(R_{ij}) = F_{ij}(R_{ij})\vec{n}_R \tag{11}$$

where R_{ij} is the distance between the two displaced atoms, and the $\vec{n}_R$ is the directional unit vector along the vector $\vec{R}_{ij}$ and it is expressed as below:

$$\vec{n}_R = \frac{\vec{r}_{ij} + \Delta\vec{u}_{ij}}{R_{ij}} \tag{12}$$

Substitution of Equation (12) into Equation (11) yields

$$\vec{F}_{ij}(R_{ij}) = F_{ij}(R_{ij})\frac{\Delta\vec{u}_{ij}}{R_{ij}} + F_{ij}(R_{ij})\frac{\vec{r}_{ij}}{R_{ij}} \tag{13}$$

Equation (13) results in a matrix expression as shown below

$$\begin{bmatrix} k & 0 & 0 & -k & 0 & 0 \\ 0 & k & 0 & 0 & -k & 0 \\ 0 & 0 & k & 0 & 0 & -k \\ -k & 0 & 0 & k & 0 & 0 \\ 0 & -k & 0 & 0 & k & 0 \\ 0 & 0 & -k & 0 & 0 & k \end{bmatrix} \begin{pmatrix} u_{ix} \\ u_{iy} \\ u_{iz} \\ u_{jx} \\ u_{jy} \\ u_{jz} \end{pmatrix} = \begin{pmatrix} F_{ix} \\ F_{iy} \\ F_{iz} \\ F_{jx} \\ F_{jy} \\ F_{jz} \end{pmatrix} \tag{14}$$

in which

$$k = \frac{F_{ij}(R_{ij})}{R_{ij}} \tag{15}$$

$$F_{ix} = -F_{jx} = \frac{F_{ij}(R_{ij})}{R_{ij}}(x_i - x_j) \tag{16}$$

$$F_{iy} = -F_{jy} = \frac{F_{ij}(R_{ij})}{R_{ij}}(y_i - y_j) \tag{17}$$

$$F_{iz} = -F_{jz} = \frac{F_{ij}(R_{ij})}{R_{ij}}(z_i - z_j) \tag{18}$$

The matrix expression in Equation (14) is computed for all atoms that interact one another and it is assembled into the system matrix consisting of all atoms' displacements. This resultant system matrix equation is nonlinear and it is solved after applying constraints. Because $\vec{R}_{ij}$ and $\vec{F}_{ij}(R_{ij})$ are unknown a priori, $\vec{u}_i$, $\vec{u}_j$ and $\vec{R}_{ij}$ are assumed initially or from the previous solution of iteration. Then, computation continues iteratively until the solution converges. The convergence criterion is the difference between the presently assumed positions and the newly computed positions of all atoms. When the difference is small enough, the solution stops.

C. COUPLING BETWEEN ATOMIC FINITE ELEMENT MODELS

Applying various boundary conditions to the atomic model is rather cumbersome. Therefore, it is beneficial to couple the atomic model with the finite element model along the boundaries of the atoms. Then, boundary conditions can be applied to the finite element model more easily. In order to combine the discrete atoms and a continuous medium, the atomic model and the finite element model of the continuous medium must be coupled properly. For simplicity, consider a two-dimensional coupling between the two models even though the same algorithm can be applied to three-dimensional bodies. Figure 4 shows atoms surrounded by a continuous medium discretized for a finite element mesh. In the figure, the inner domain is the atomic domain while the outer domain is the finite element domain of continuous medium. The intermediate domain bounded by bold lines is called interface domain where both atoms and finite element meshes overlap each other.

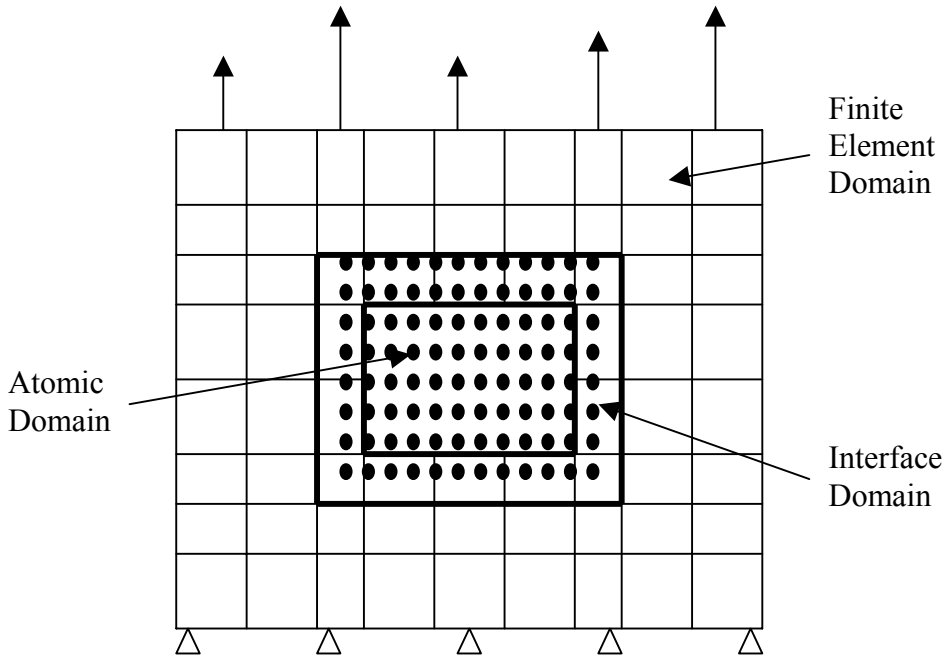

Figure 4. Coupling between atomic and finite element domains

The atomic and finite element models are solved independently in a staggered manner. The solution procedure for the coupled problem is explained below:

1. Solve the finite element domain equation $[K_f]\{u_f\} = \{F_f\}$. From now on, subscripts *f* and *a* denote finite element and atomic solutions, respectively.
2. Compute the embedded atoms' displacements from the finite element nodal displacements using the finite element shape functions such as $\{u_a^e\} = [N]\{u_f^e\}$ where superscript *e* indicates the embedded atoms or finite elements containing such atoms, and $[N]$ is the shape function matrix of finite elements.
3. Compute the new positions $\{x_a^e\}$ of the embedded atoms by adding the displacements computed above to the previous positions.
4. Solve for the rest of atoms' new positions with fixed embedded atoms' positions using the atomic model.
5. Compute the interactive forces $\{F_a^e\}$ on the embedded atoms exerted by all atoms.
6. Compute the equivalent nodal forces of the finite elements containing the atoms using $\{F_f^e\} = \int_{V^e} [N]^T \{F_a^e\} dV$ where V^e is the element volume containing atoms.
7. With the nodal forces computed above, the new finite element solution is obtained. Then, continue the process from Step 2.

III. NUMERICAL RESULTS AND DISCUSSION

A. ATOMIC MODEL ONLY

1. Square and Hexagonal Atom Array with Hole at the Center

a. Square Atom Array with Hole at the Center

Figure 5 shows a two-dimensional 21x21 square array of atoms with vacancies of atoms at the center. The atoms on the four boundaries could move tangentially along the boundary but not perpendicularly. Figure 5(a) shows our initial square atom array with atoms removed at the center. Figure 5(b), 5(c) shows that the atoms are moving in the downward direction to satisfy the potential equilibrium under the constraints of fixed bottom atoms. The arrows in Figure 5(b) indicated the directions and magnitudes of the movement of each atom. The equilibrated position of atoms is shown in Figure 5(c)

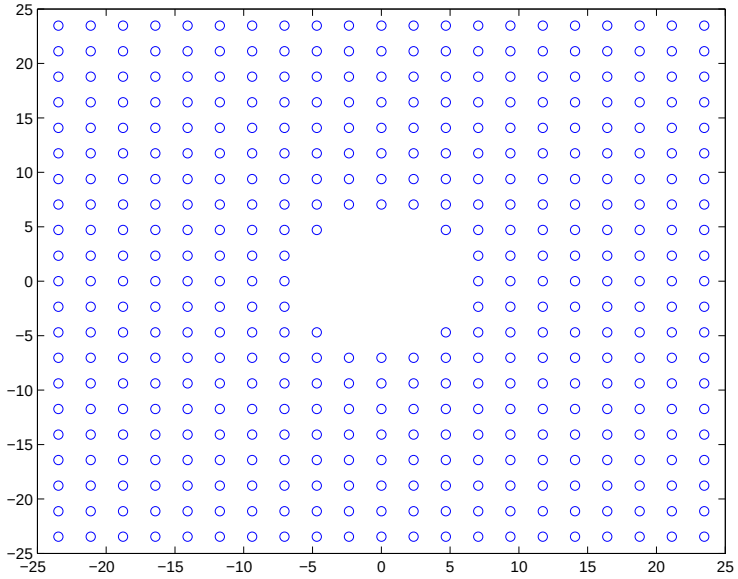

(a) Initial array with a hole

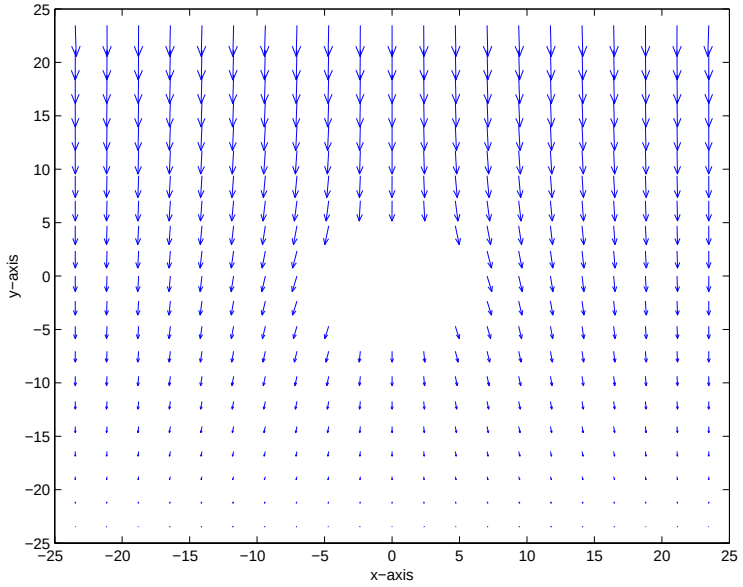

(b) Movement for equilibrium

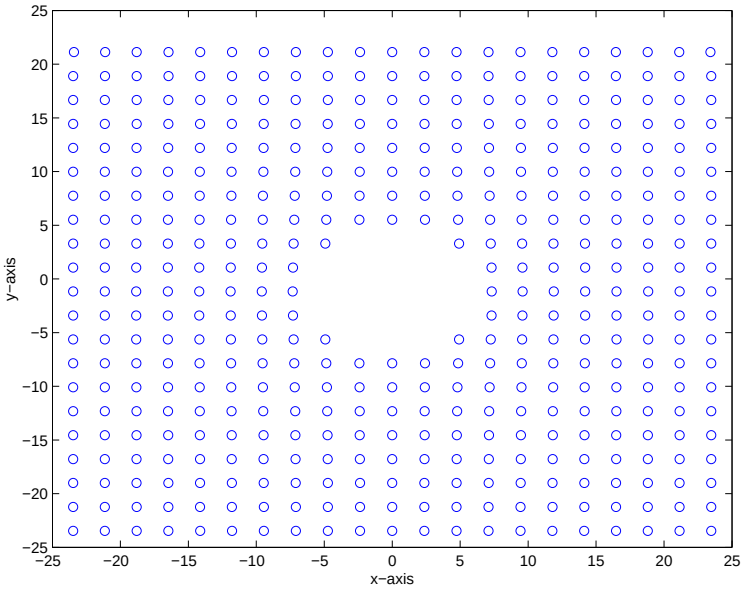

(c) Equilibrated position of atoms

After that equilibrium state, the atoms look for the new equilibrium position as the top boundary is incrementally displaced uniformly in the upward direction as shown in Figures 5(d) through 5(e). After the movement of each atom shown in Figure

5(d), Figure 5(e) shows that the new equilibrated position of atoms under upward displacement. As shown in Figure 5(e), some amount of movement of atoms in upward direction can be examined due to the applied displacement in upward direction.

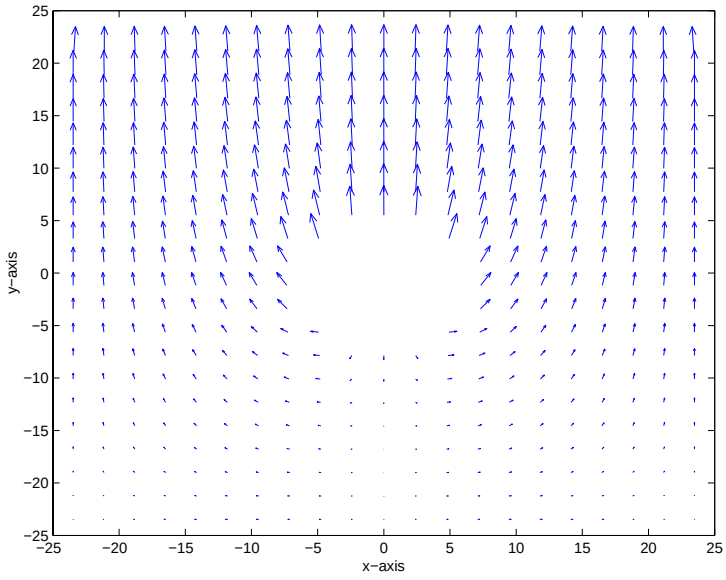

(d) Upward displacement

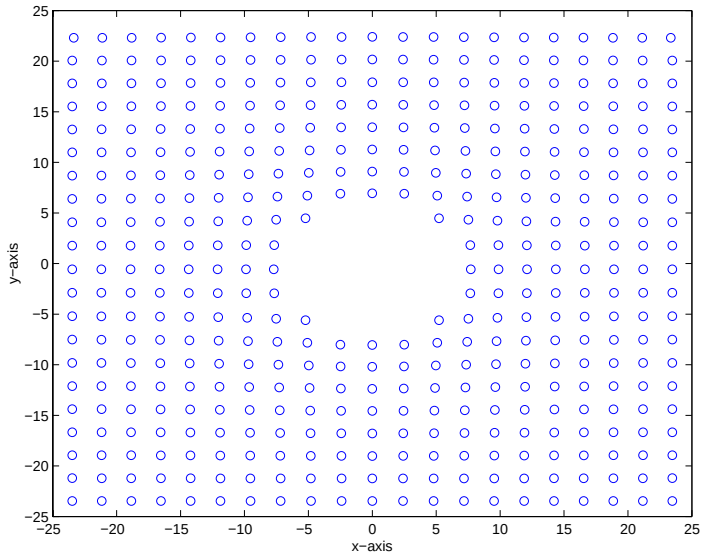

(e) New equilibrated position of atoms

Figure 5. Square array of atoms with a hole.

b. Hexagonal Atom Array with Hole at the Center

Figure 6 shows a two-dimensional 41x41 hexagonal array of atoms, which is much more similar to real atom array than square one, with vacancies of atoms at the center. The boundary conditions and the number of atoms are the same as the ones of square array case. Figure 6(a) is the initial array of atoms. The number of atom was increased to see difference with 21x21 square atom array in atomic behavior. As shown in Figure 6(b), the atoms have shrunk down in downward direction to satisfy the potential equilibrium and went to the equilibrium state like Figure 6(c). As we did in square atom array, the upward displacement was placed to the top atom line. The atomic behavior was generally similar to the one of the 21x21 square atom array as shown Figure 6(d), 6(e). The arrows in Figure 6(b), (d) tells the direction and magnitude of movement of atoms in hexagonal array.

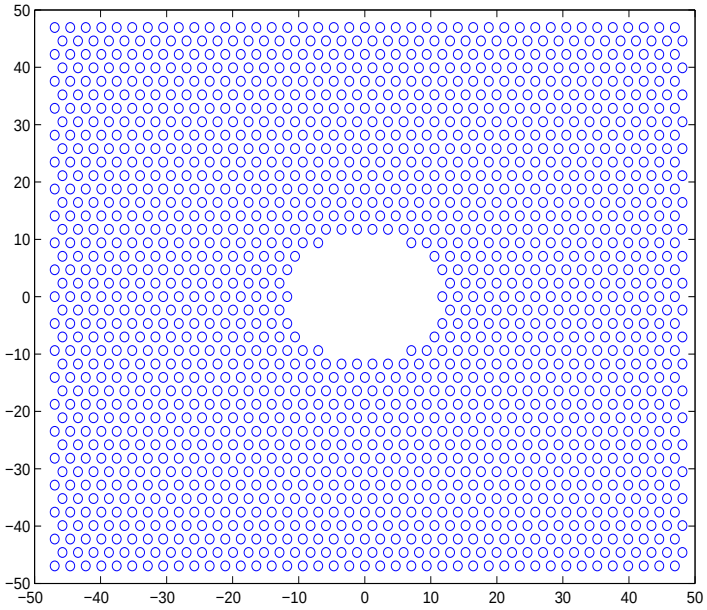

(a)

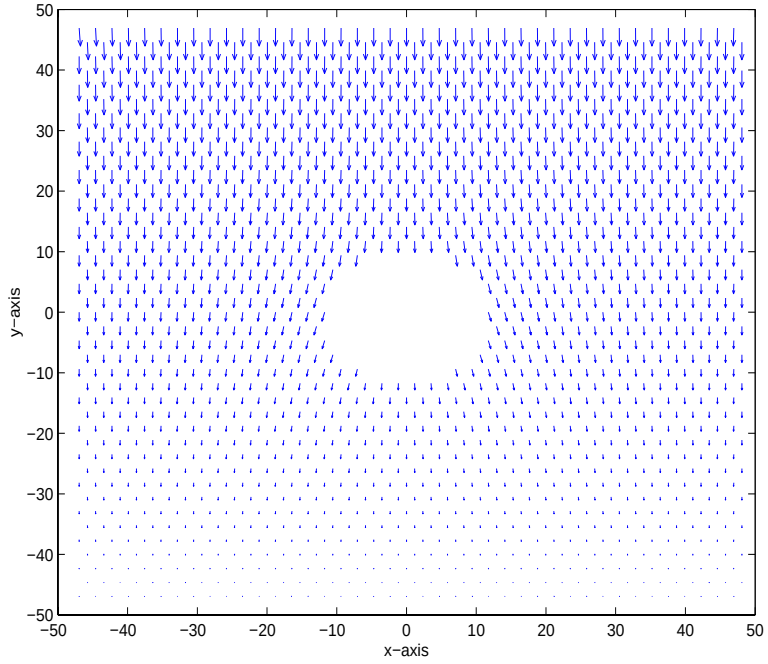
y−axis
x−axis
50
40
30
20
10
0
−10
−20
−30
−40
−50
−50
−40
−30
−20
−10
0
10
20
30
40
50

(b)

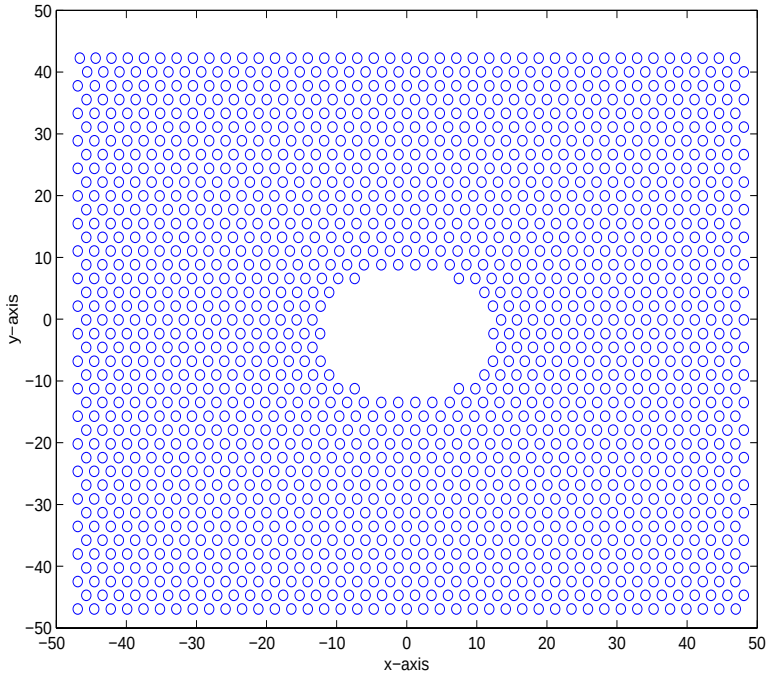
y−axis
x−axis
50
40
30
20
10
0
−10
−20
−30
−40
−50
−50
−40
−30
−20
−10
0
10
20
30
40
50

(c)

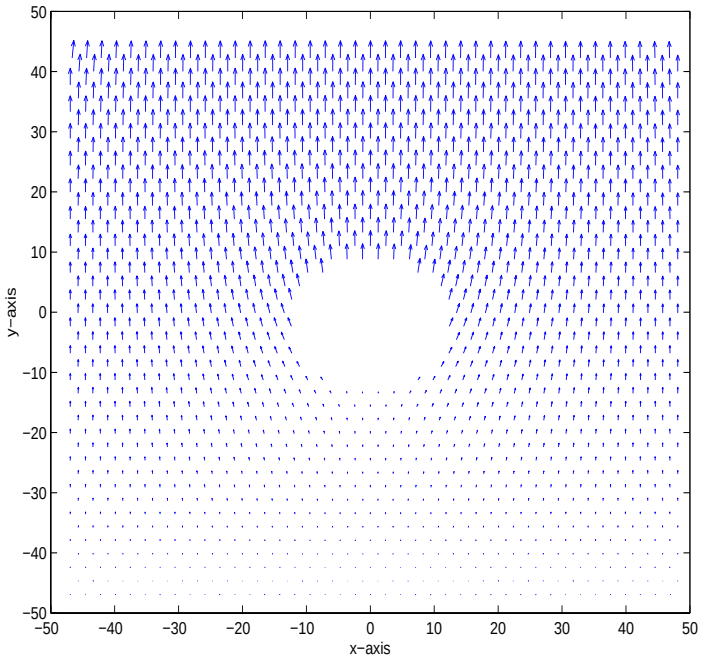

(d)

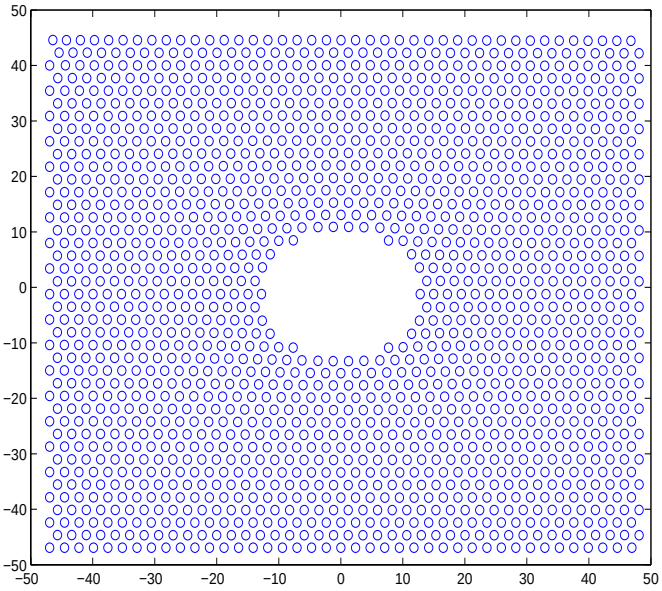

(e)

Figure 6. Hexagonal array of atoms with a hole.

2. Square Atom Array with Dislocation

Figures 7(a), 8(a), 9(a) show initial equlibriums of atoms with a dislocation oriented in 27, 45, 63 drgrees respectively to the horizontal axis. The boundary and loading conditions were the same as the hole case.

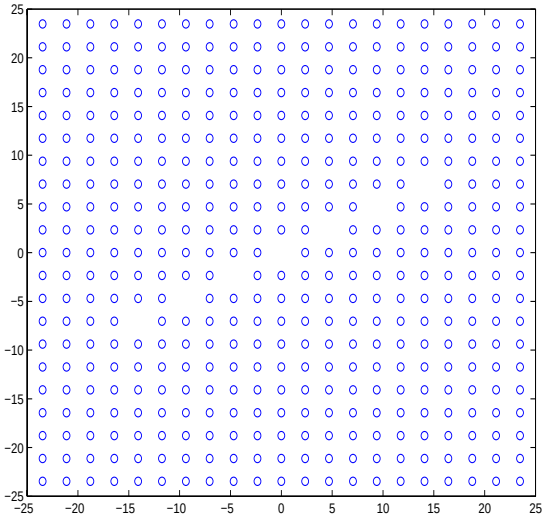

(a)

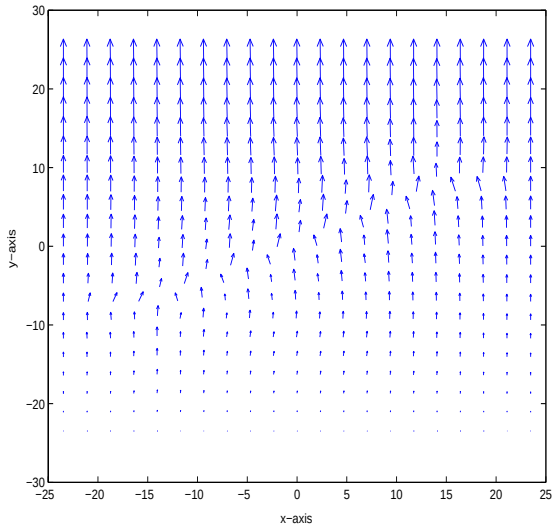

(b)

Figure 7. Square array of atoms with a dislocation with 27 degree orientation.

As the tensile load is applied in the vertical direction at the top boundary, the displacements of atoms into the new equilibrium in each case are depicted in Figures 7(b), 8(b), 9(b). These figures illustrates how a slanted dislocation affects the movement of atoms under a uniform load.

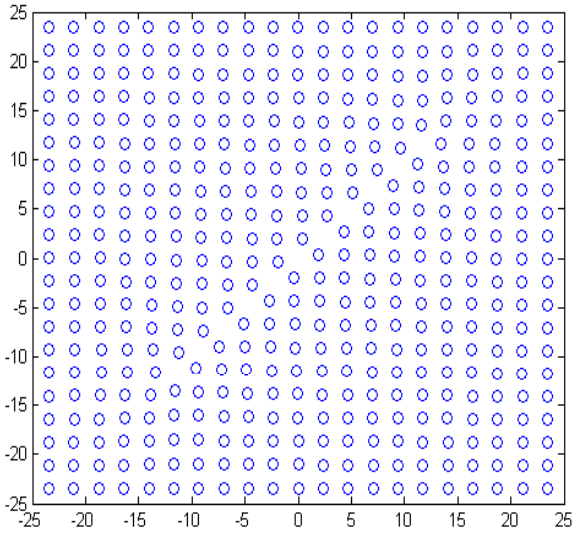

(a)

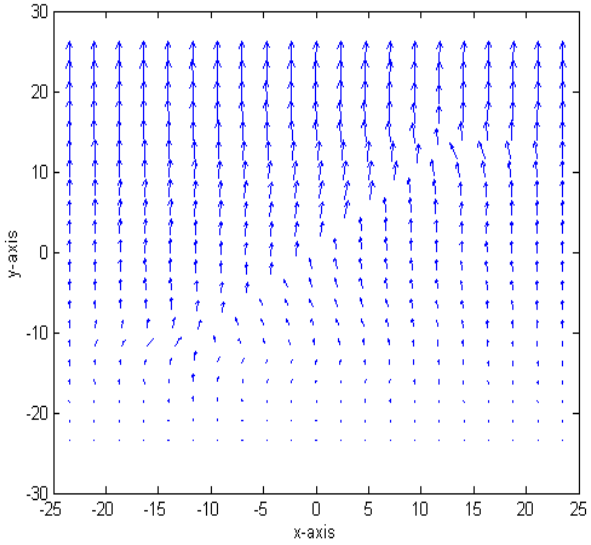

(b)

Figure 8. Square array of atoms with a dislocation with 45 degree orientation.

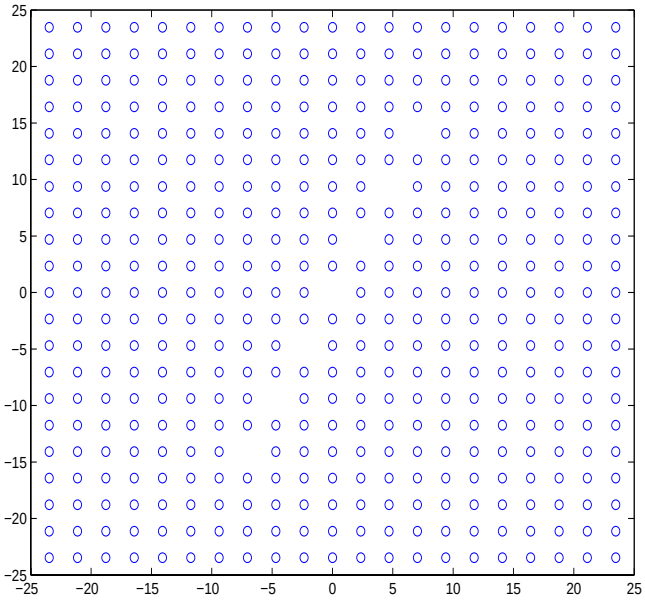

(a)

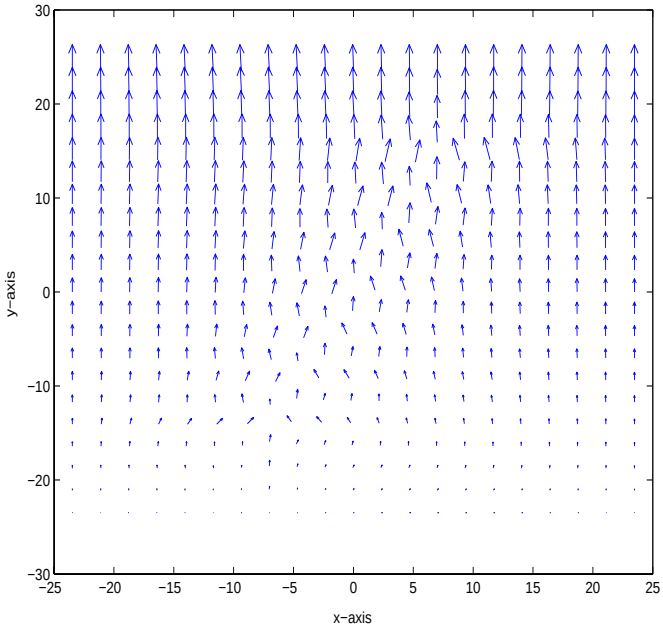

(b)

Figure 9. Square array of atoms with a dislocation with 63 degree orientation.

3. Square Atom Array with Hole and Dislocation

Figure 10(a) shows that the initial 31x31 square atom array with hole and dislocation of 45 degrees direction to the horizontal.

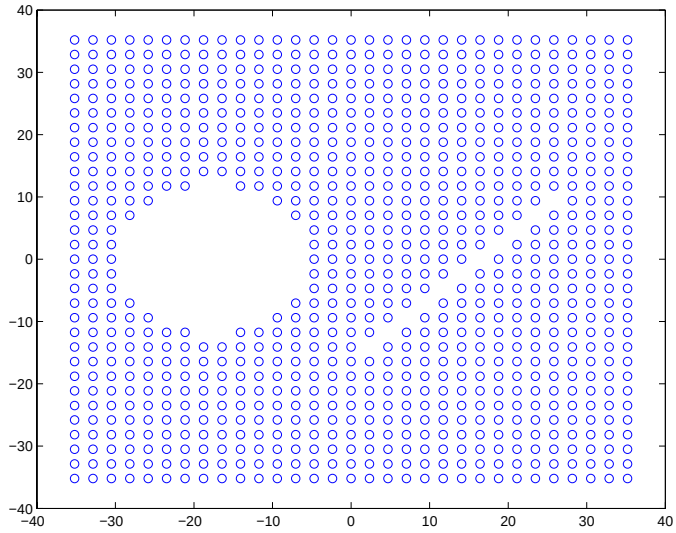

(a)

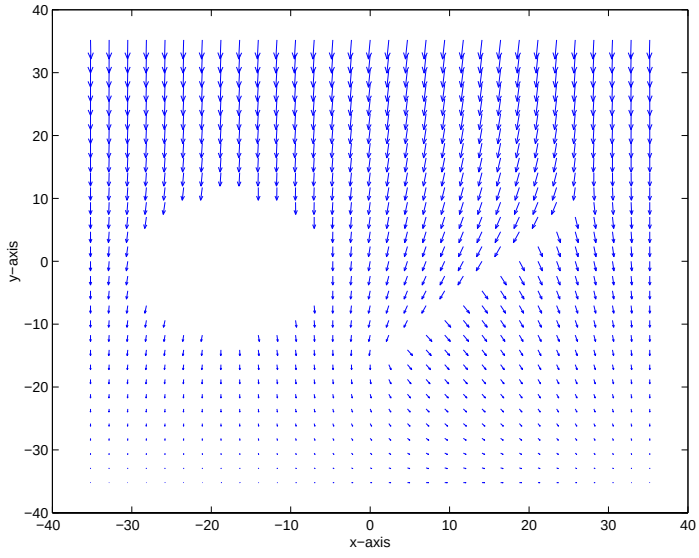

(b)

To find equilibrated position of atoms, the potential energy function was used. The arrows in Figure 10(b) show the movement of atoms to reposition their sites and Figure 10(c) shows the equilibrated position.

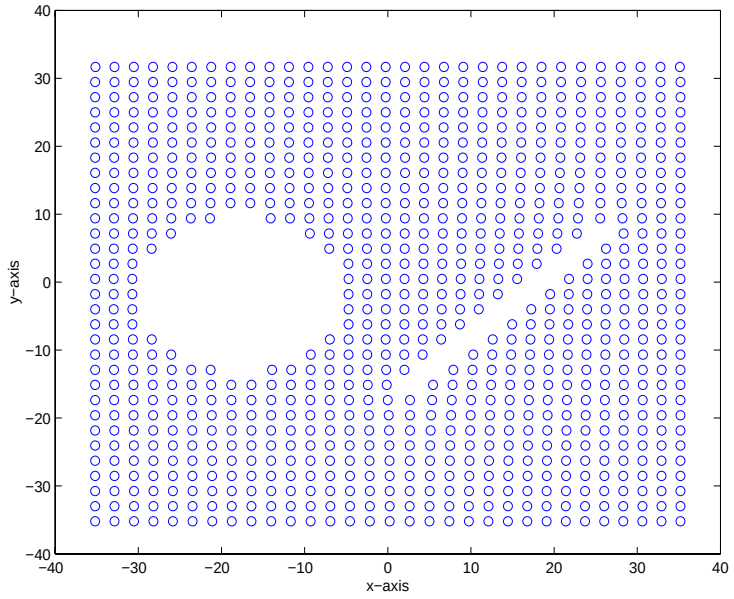

(c)

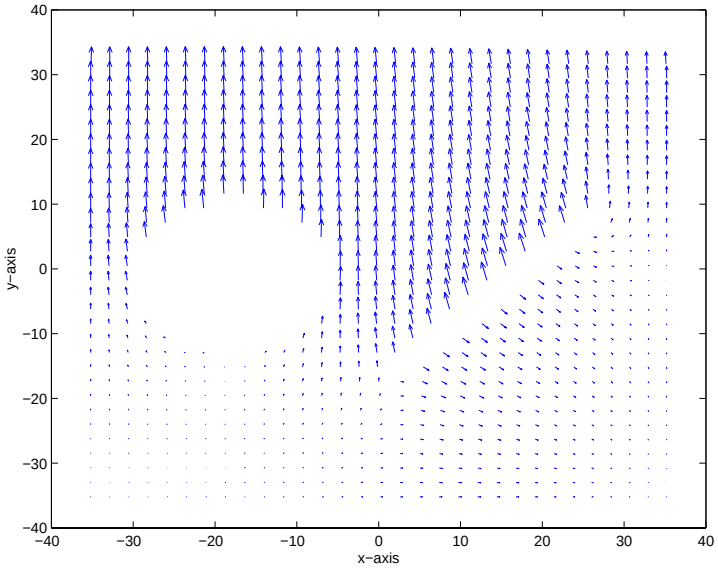

(d)

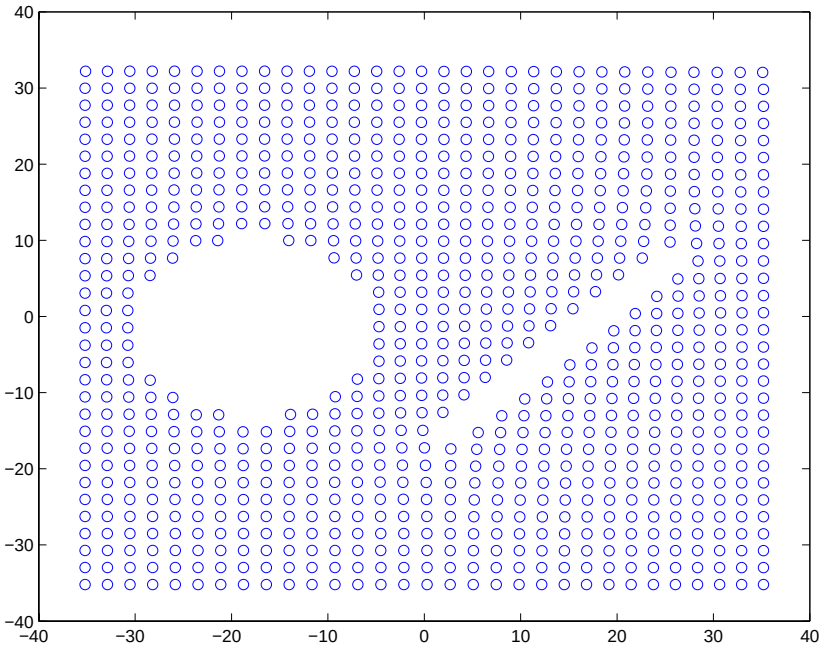

(e)

Figure 10. Square array of atoms with a dislocation and a hole.

As shown in Figure 10(e), it indicates the new equilibrated array after the upward direction displacement is applied to the equilibrated state. It can be examined that the some amount of displacement of the array in upward direction due to the applied displacement.

4. Square Atom Array with a Notch

Figure 11 shows the case of square atom array with a notch. Figure 11(a) is the initial array of atoms in which the atoms on the left-side and bottom line boundaries are constrained from normal displacements to the boundaries and all other atoms are free t to move. Figure 11(c) shows the final array of atoms after the movement of atoms to satisfy the equilibrium of potential of atoms while Figure 11(b) shows the movement of atoms during that process. In Figure 11(d), arrows indicate movements of atoms as the top boundary is displaced uniformly in the upward direction. It can be seen that atoms above the notch are moving larger than the ones below the notch, which means that the notch is

getting increased with the applied displacement. Figure 11(e) shows the final array of atoms after movements.

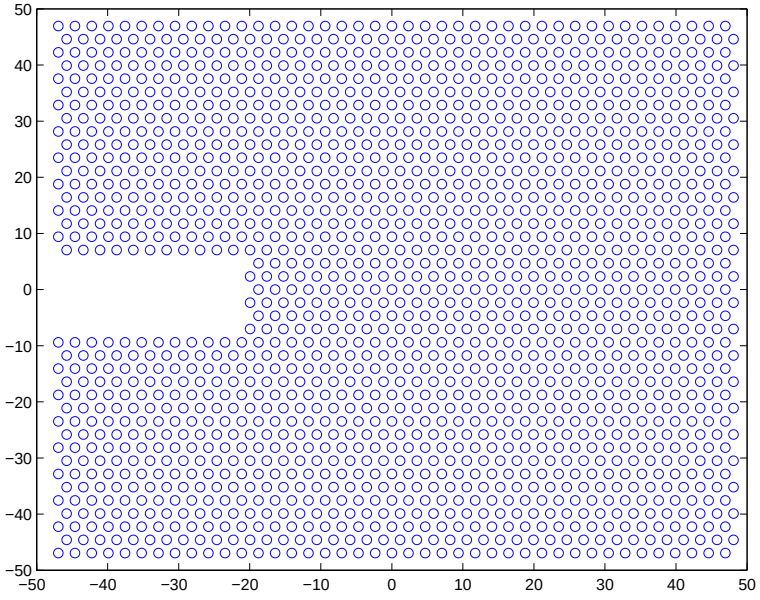

(a)

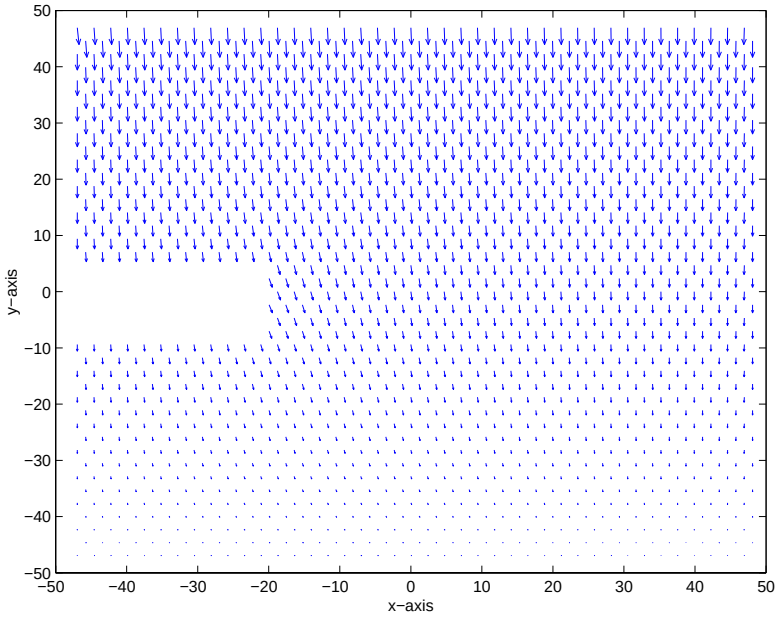

(b)

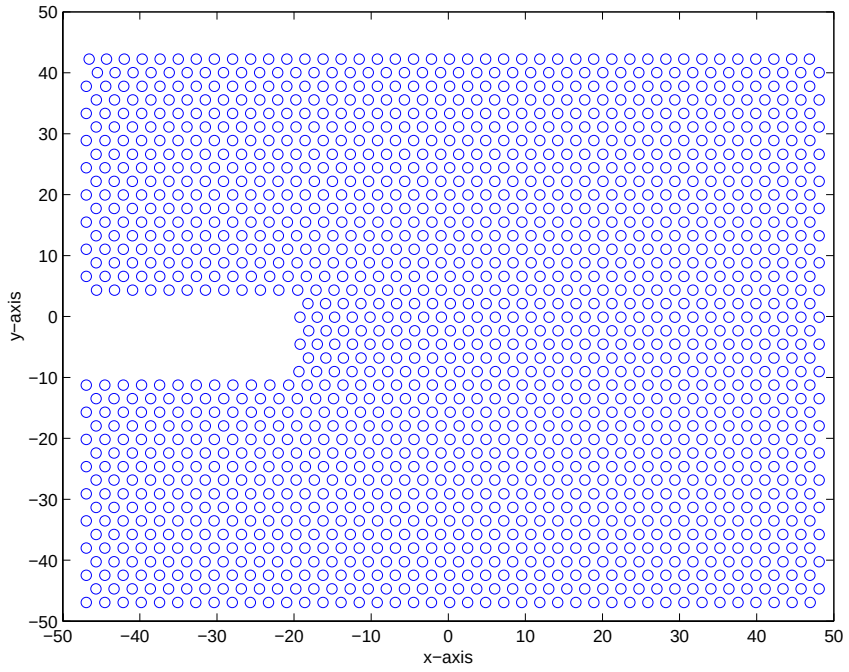
50
40
30
20
10
0
−10
−20
−30
−40
−50
y−axis
−50 −40 −30 −20 −10 0 10 20 30 40 50
x−axis

(c)

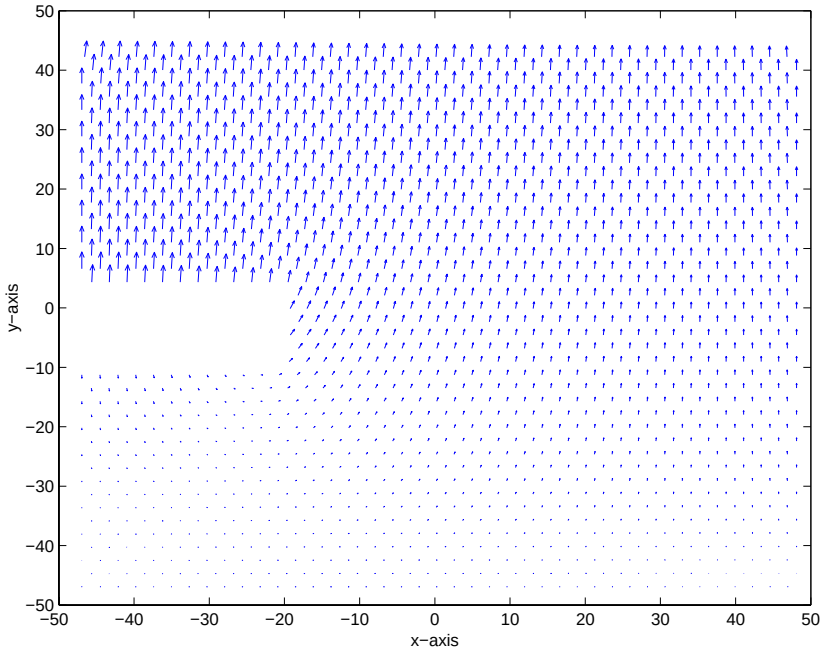
50
40
30
20
10
0
−10
−20
−30
−40
−50
y−axis
−50 −40 −30 −20 −10 0 10 20 30 40 50
x−axis

(d)

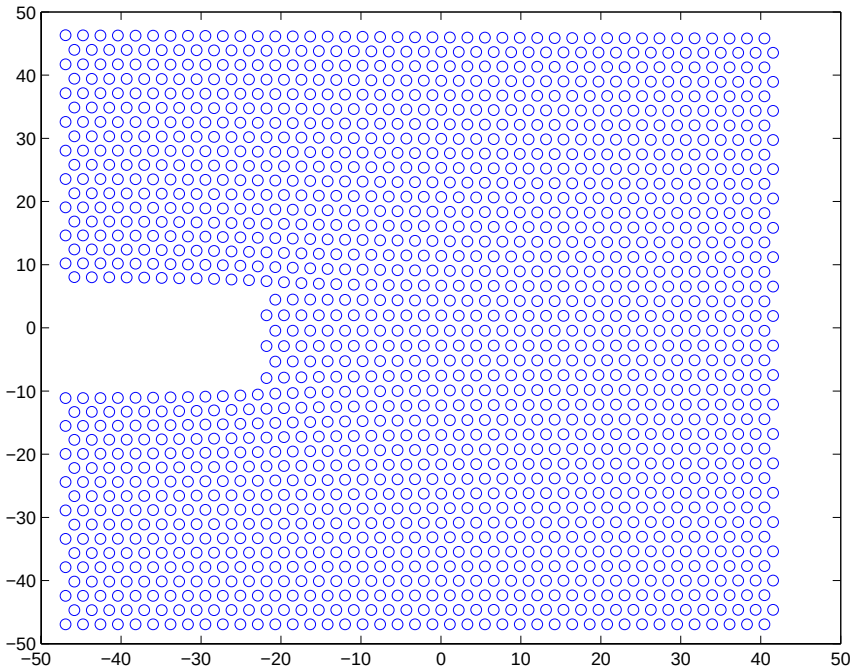

(e)

Figure 11. Square array of atoms with a notch.

B. COUPLED MODEL OF ATOMIC AND FINITE ELEMENT MODEL

1. Hexagonal Array of Atoms with a Dislocation

For the coupled model, uniform shear or axial force was applied at the top of the finite element model. Figure 12(a) shows the atoms surrounded by the finite element mesh. The finite element mesh makes easy to apply loading and constraint boundary conditions. In order to model dislocation, a small number of atoms were removed at the center. Figure 12(b) is the initial equilibrium positions of atoms. Figures 12(c) through 12(e) shows the movement of atoms under shear, tensile, or compressive load respectively. The displacements of atoms were magnified in the arrow plots. Therefore, the final positions of atoms are not at the tip of the arrows. Figure 12(f) shows the final atomic positions with the applied shear load associated with Figure 12(a). Arrows indicate movements of atoms as the top boundary is displaced uniformly in the upward direction.

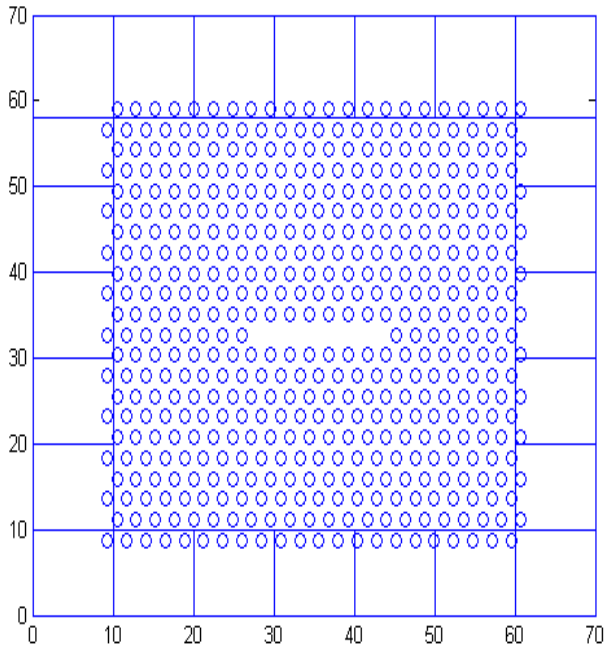

(a) Initial coupled model with dislocation.

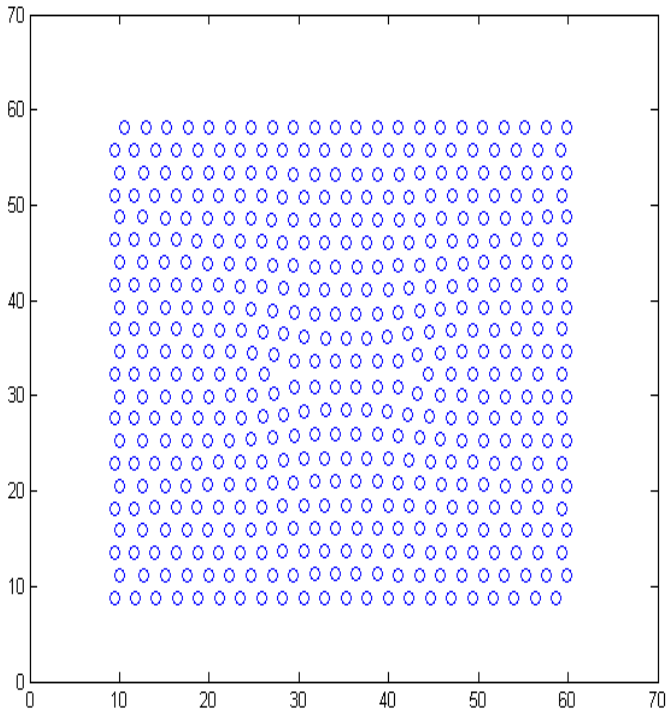

(b) Equilibrated positions

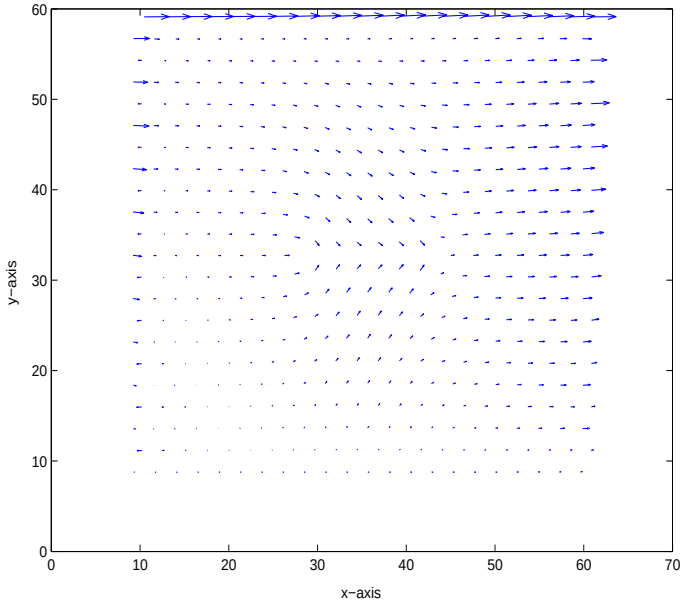

(c) Shear load.

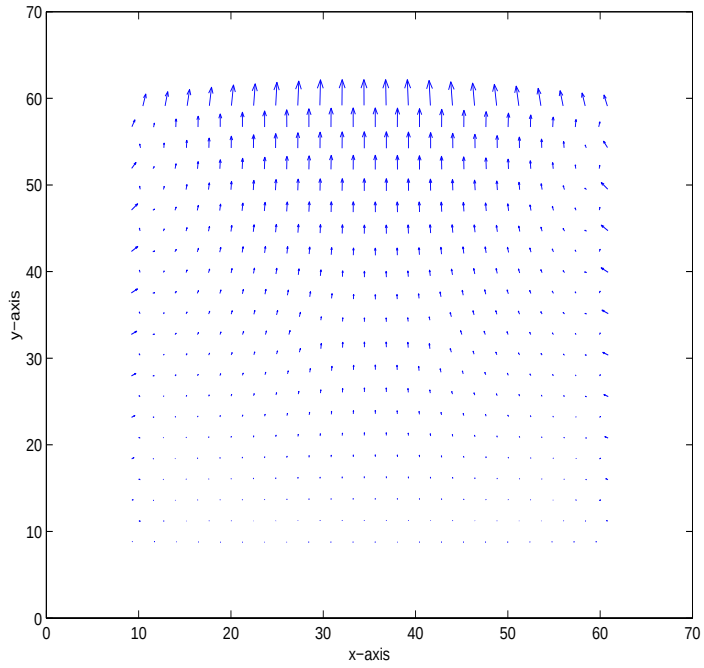

(d) Tensile load.

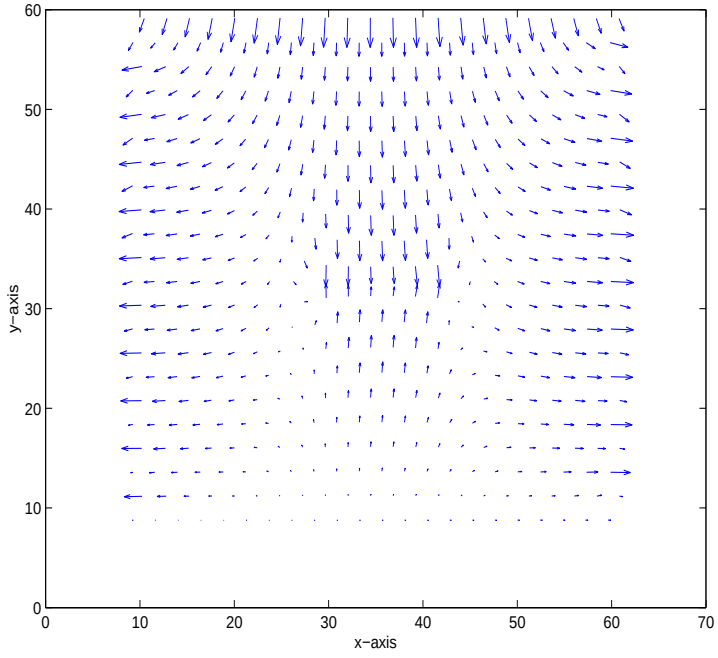

(e) Compressive load.

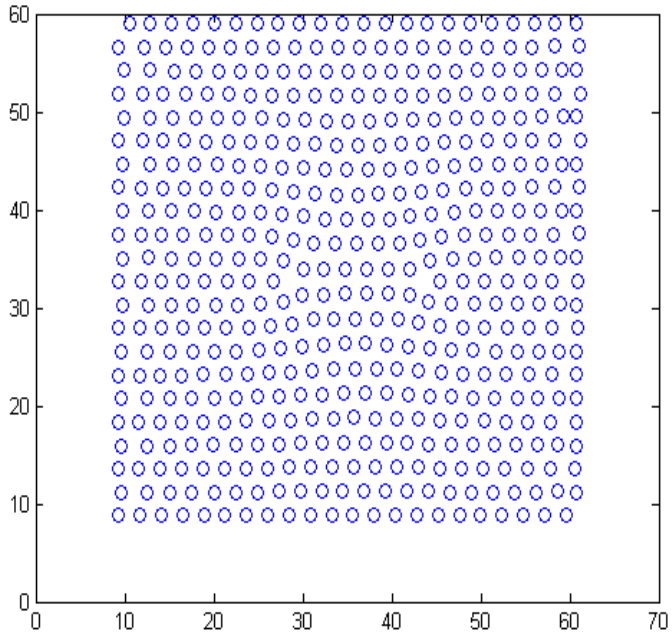

(f)Atomic positions with the shear load

Figure 12. Hexagonal array of atoms with a dislocation.

2. Atomic Array Embedded in the Finite Element Mesh with a Crack

The model studied the atomic behavior at the tip of a crack. The atomic model is embedded inside the finite element analysis model at the crack tip location as shown in Figure 13. Two different shapes of atomic arrays were considered: square and hexagonal arrays. The finite element domain was constrained at the bottom edge and uniformly stretched at the top edge. In other words, the problem was the uniaxial tensile loading case. Displacements of atoms at the notch tip zone are plotted in Figures 14 and 15 for the square and hexagonal arrays, respectively. In those figures, the atomic displacements were plotted relative to those of the atom at the crack tip, which was located at the origin of the coordinate system, i.e. (0,0). Therefore, the crack tip displacement was zero. Because of symmetry, a half of the atomic domain was plotted in those figures. There was a very minor difference between the two arrays of atoms. Therefore, the atomic arrangement barely affected the atomic displacements. Both figures clearly show larger vertical displacements of atoms, as they get closer to the notch tip position. For

comparison, the displacements very near the crack tip in a continuous body are illustrated in Figure 16. The atomic displacements and continuum displacements were qualitatively similar even if there were differences in details.

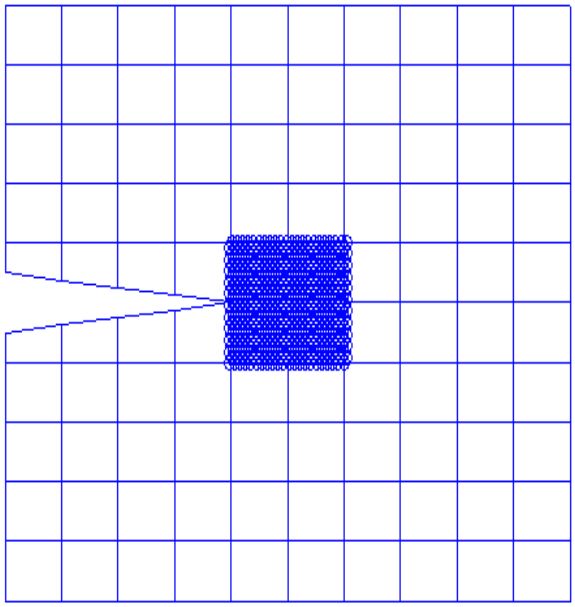

Figure 13. Atomic Array Embedded in the Finite Element Mesh with a Crack

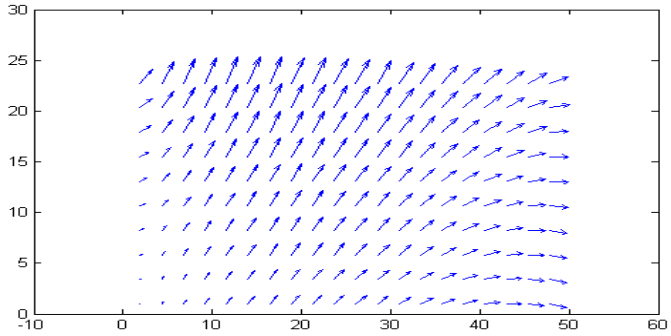

Figure 14. Atomic Displacements in a Square Array Near the Crack Tip

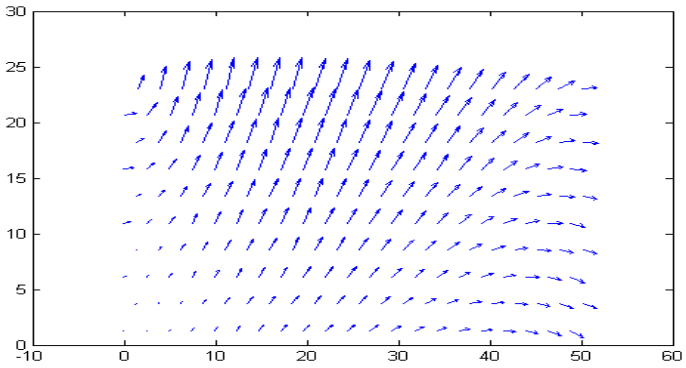

Figure 15. Atomic Displacements in a Hexagonal Array Near the Crack Tip

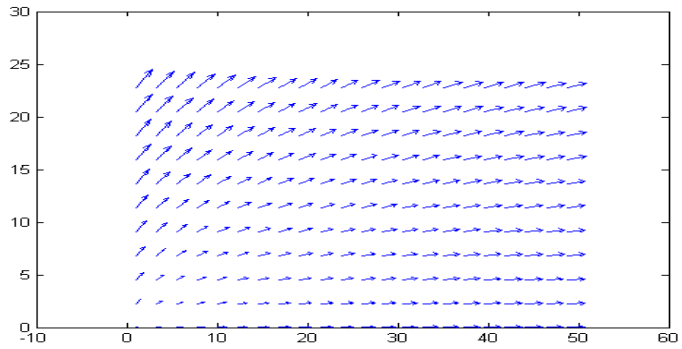

Figure 16. Displacement Field Near the Crack Tip in a Continuous Medium

3. Atomic Behavior at the Crack Tip

The atomic behavior was examined with some vacancies of atoms at the crack tip. Figure 17 shows the embedded atoms in a finite element mesh. An edge crack is shown in the figure and the atoms are located around the crack tip. The two left bottom nodes were constrained while the left top nodes were subject to tensile force.

The initially equilibrated atoms before external loading is shown in Figure 18. Then, tensile load was applied at the left side of the model like a compact specimen under tensile load. In other words, tensile forces were applied to the top left nodes while constraint of movement was applied to the bottom left nodes. Figure 19 is the plot for atomic movement with the tensile load and the final atomic positions in equilibrium with the external load. It was examined that there was a small size of crack at the bottom site

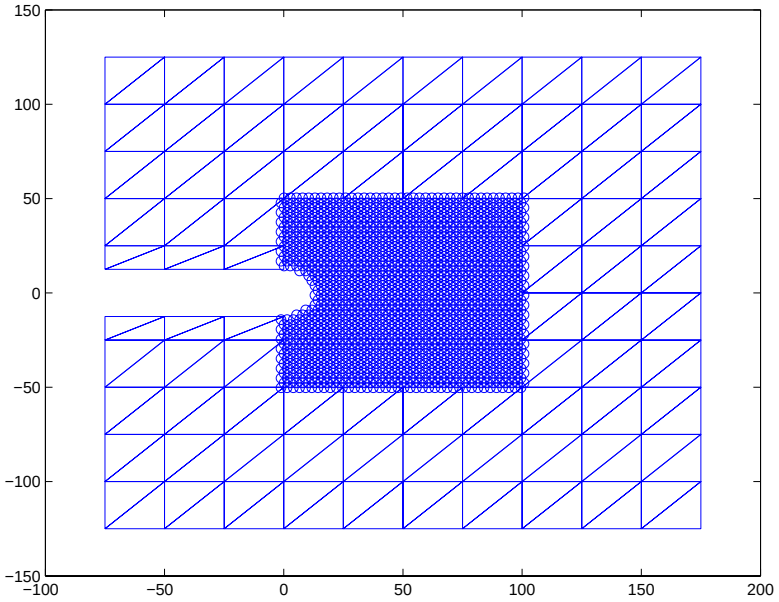

Figure 17. Atomic and Finite Element Model with a Crack

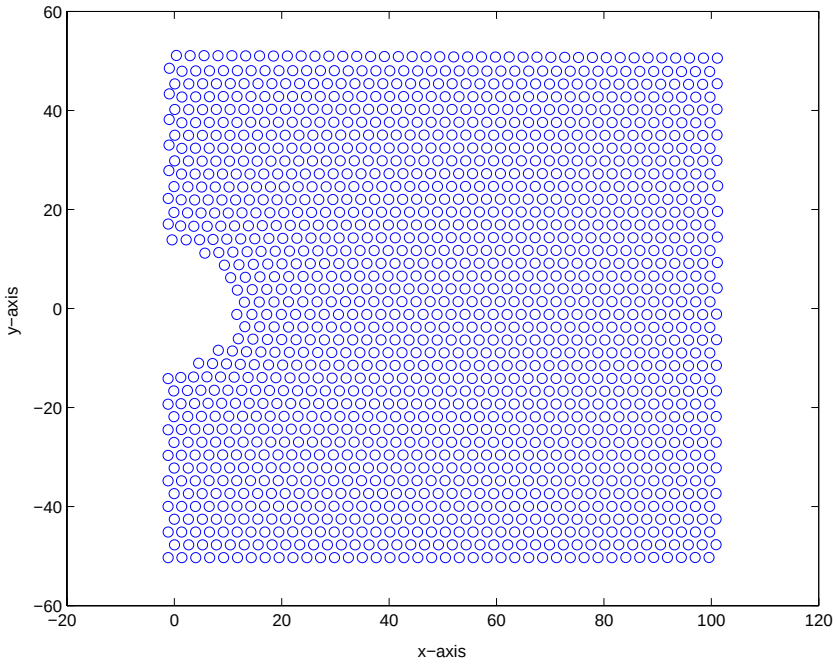

Figure 18. Initial Equilibrium Positions of Atoms

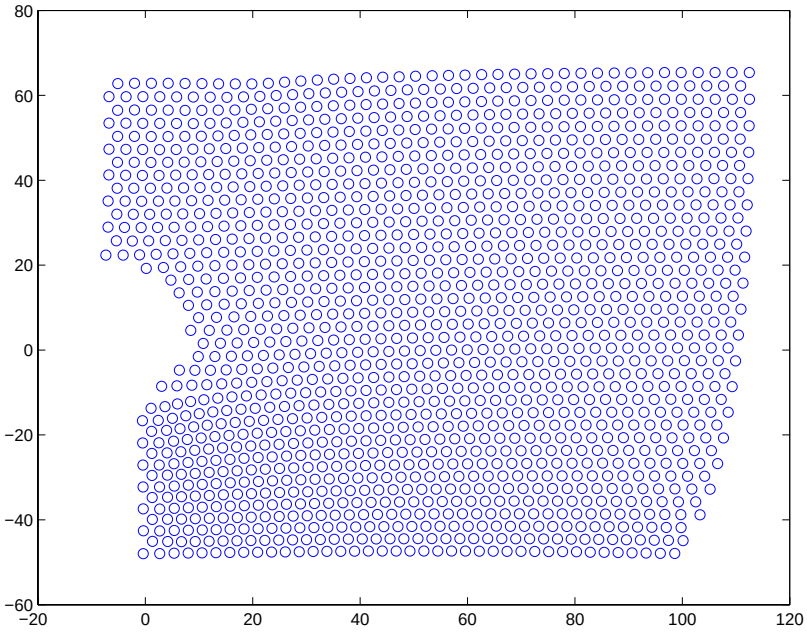

Figure 19. Movement of Atoms with Tensile Opening Force

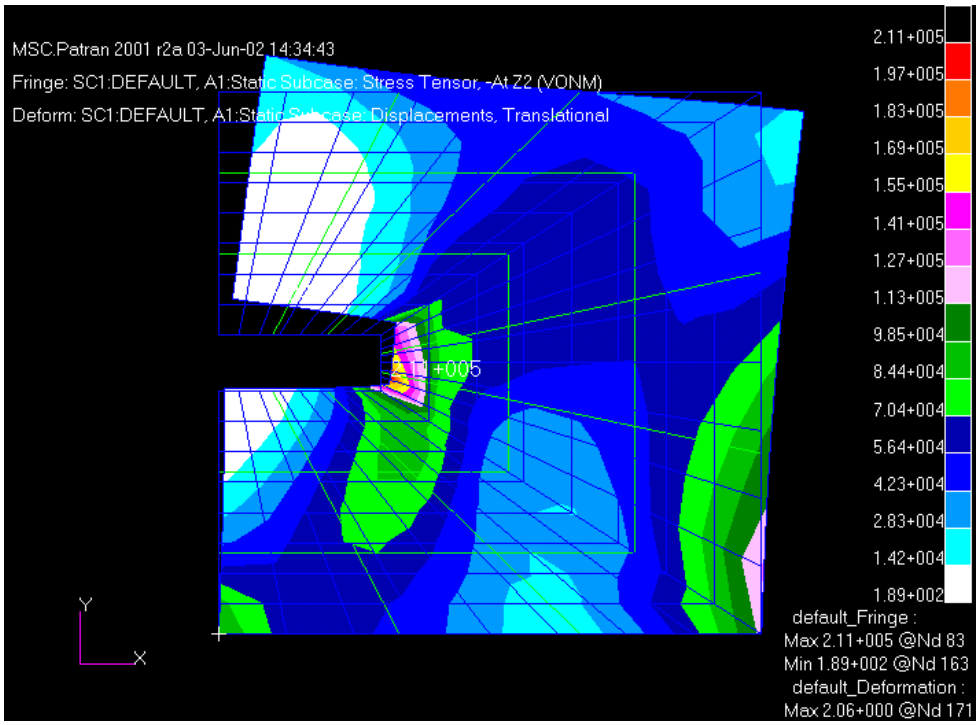

Figure 20. Final Equilibrium Positions of Atoms with Tensile Opening Force

of the notch tip because of the stress concentration at that point. To see if there is stress concentration at that point in a continuous medium, a commercial program, MSC PATRAN/NASTRAN was used. As shown in Figure 20, the highest stress point exactly corresponds to the one of our developed model, which means that the atomic behavior in nano-scale is quite comparable to the one in the continuum material.

C. ESTIMAION OF EFFECTIVE STIFFNESS OF NANOTUBES

1. Armchair Nanotube

As mentioned in background section, we consider two types of nanotubes, which are armchair and zigzag. One armchair nanotube is shown in Figure 21(a) below. Figure 21(b) is our initial armchair model of (6,6) SWNT that has the closing atom arrays at both sides of tube. Then one atom at the bottom was fixed in all direction to prevent the rigid body motion of nanotube and the other atom at the top section is fixed at x-y direction and free to go z-direction.

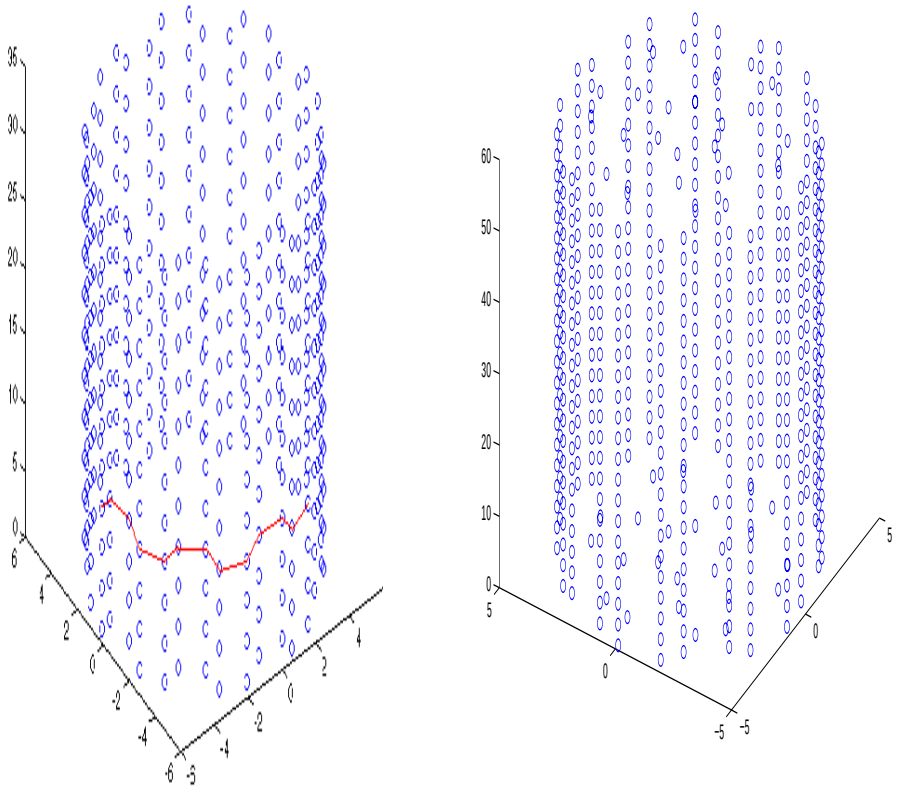

(a) (b)

Figure 21. Armchair nanotube model

From the Tersoff-Brenner potential function, the equilibrium state of our initial armchair model is presented in Figure 22(a). It is noticed that the entire size of the tube

has decreased to satisfy the potential equilibrium among atoms. After the atomic equilibrium state, the axial tension force was applied to the atoms at the top circle in z-direction. As a result of the force, it was examined that the nanotube had some elongation due to that tension force in some amount of length as shown in Figure 22(b). From that elongation, the effective stiffness of our nanotube model could be calculated as below.

$$E = \frac{\sigma}{\varepsilon},$$

where $\sigma = \frac{Force}{Area}$ and $\varepsilon = \frac{\Delta l}{l}$ where Δl is the elongated length of tube and l is initial length of the tube.

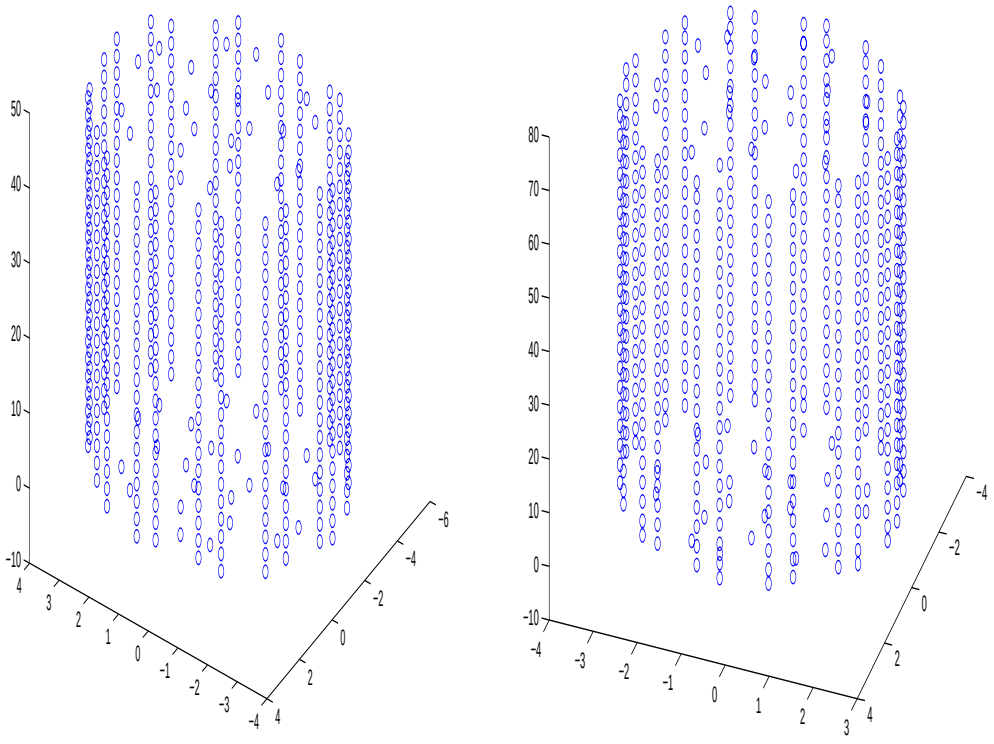

(a) (b)

Figure 22. (a) Armchair nanotube in equilibrium, (b) Elongated nanotube

Using the equation above, Young's modulus of our armchair carbon nanotube model can be found along tube axis. The estimated modulus value of the tube ranged around 1.0 Tpa for (6,6) chiral vector. Compared to Young's moduli values from other simulation techniques such as classical MD, ab initio method, or the experimental estimation, the modulus value from our simulation was quite close to those values that range from 1 to 1.2 Tpa. Furthermore, the nanotube model that has 12 circumferential atoms was developed as shown Figure 23(a) and 23(b) so that the radius of the carbon nanotube can be changed, which allowed

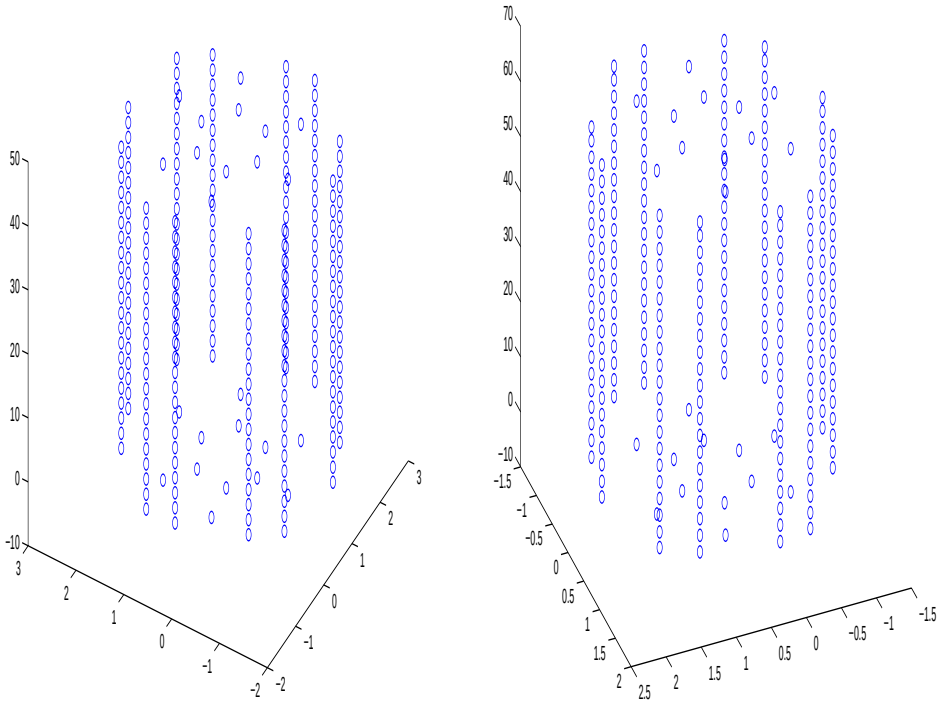

(a) (b)

Figure 23. (a) 12 atom circumference in equilibrium, (b) Elongated nanotube

us to get the different modulus value. And it was noted that the modulus of nanotube was getting decreased with decrease of the radius of the nanotube. A previous research stated that Young's modulus of CNT is slightly dependent on the tube size especially for small

diameter nanotubes (D<1.2nm) [reference2], our results are quite corresponding to those results. In other words, the modulus increases with increase of tube diameter.

2. Zigzag Nanotube

The other type of nanotube is the zigzag that is shown in Figure 24(a), which has the chiral vector of (12,0). Figure 24(b) is initial simulation model. The atoms for the top and bottom of the tube were filled in same way as the previous armchair SWNT and the constraints are the same as well. From the same way of finding the modulus of armchair nanotube, the predictable modulus of the model was about 1.40 Tpa for (12,0) SWNT, which is quite similar to the one of the (6,6) SWNT.

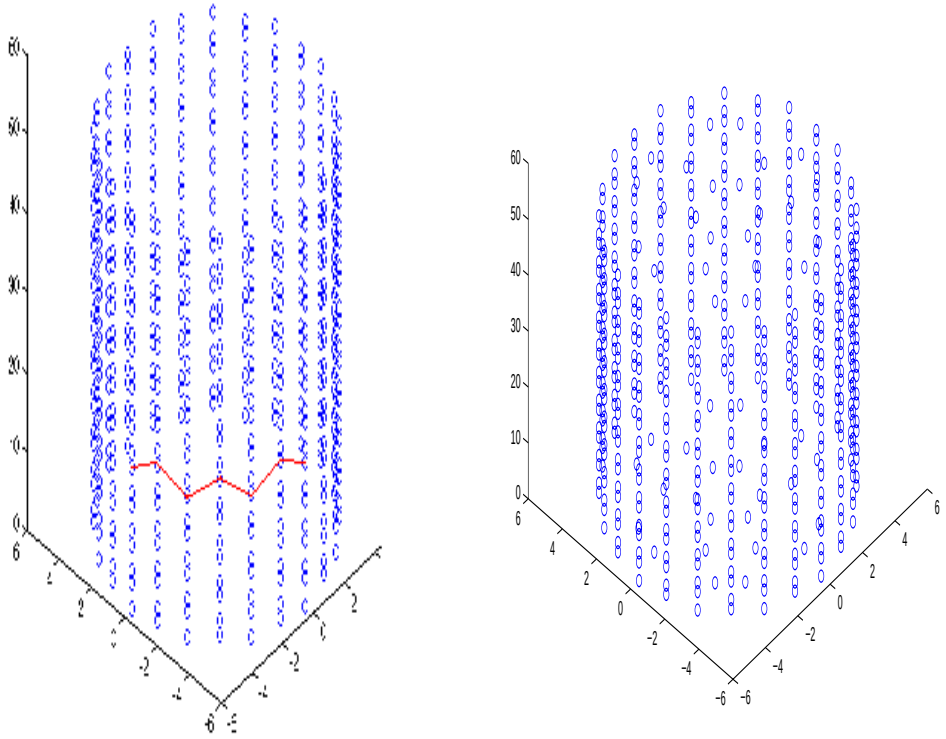

(a) (b)

Figure 24. Zigzag SWNT model

Also, for the small size of zigzag SWNT, (6,0) SWNT that has 12 circumferential atoms was modeled and approximately Young's modulus of 1.1 Tpa was

investigated. Compared to other studies, it corresponds to the result that the young's modulus slightly increases with the tube diameter.

D. MULTI-SCALE ANALYSIS OF A COMPOSITE STRUCTURE MADE OF CARBON NANOTUBES

The last example used a multi-scale analysis of a composite structure made of carbon nanotubes as illustrated in Figure 25. Fibers were assumed to be composed of bundles of single-walled nanotubes and the fiber strands were woven to a fabric. The composite structure was made of multi-layers of the fabrics in various orientations. The present example was to compute the effective material properties of the woven-fabric composite lamina. Two different types of woven fabrics were considered. One was the plain-weave fabric and the other was the 2/2-twill weave fabric.

As shown in previous section, the modulus of SWNT depends on the radius of tube. So it is assumed that the SWNT of (12,0) chiral vector is used for the woven-fabric composite. At the next step, long continuous fibers were fabricated from the nanotubes. Then, the longitudinal elastic moduli of the unidirectional composite were 750 GPa using the fiber-strand model as provided in [22] with an assumption of 50% fiber volume. The elastic moduli of the plain weave composite made of the strands were computed as 360 GPa in the inplane direction using the strand-fabric model [23]. The same strands were used in both fill and warp directions. The 2/2-twill composite woven using the same fiber and matrix materials had the elastic moduli of 220 GPa in the inplane.

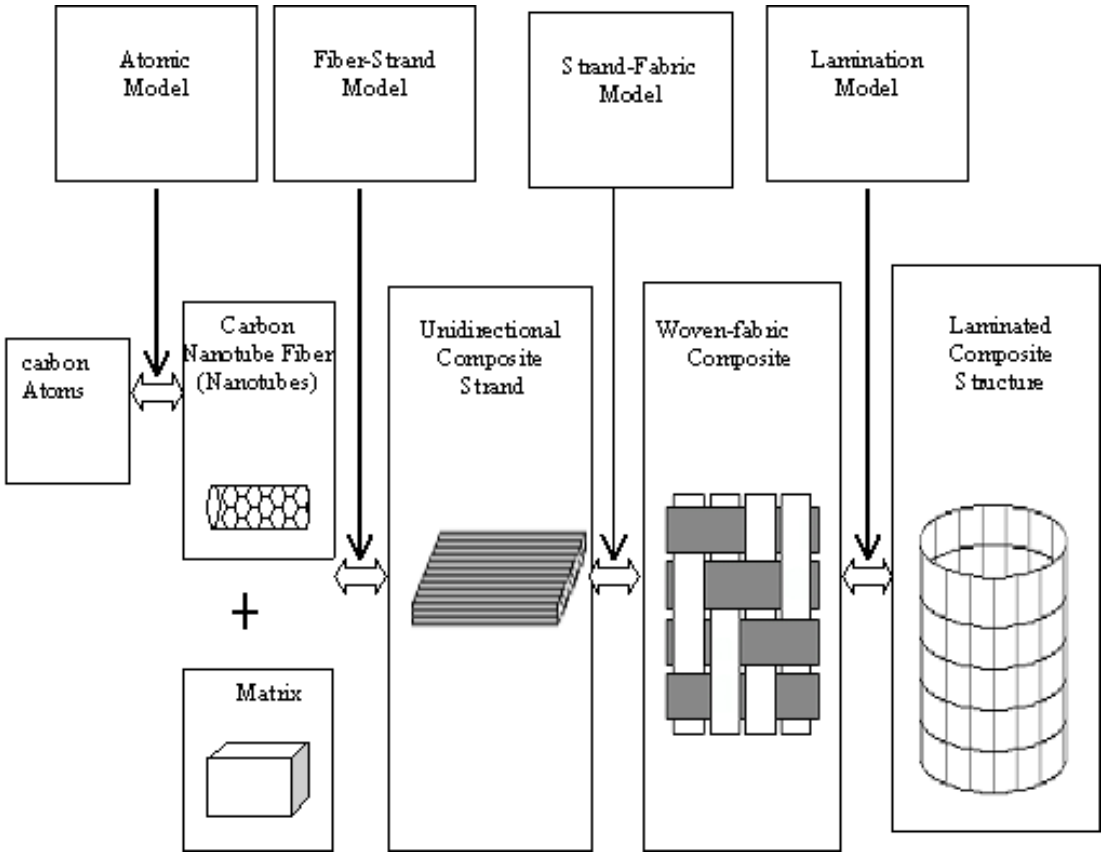

Figure 25. Multi-scale analysis of a laminated composite structure

THIS PAGE INTENTIONALLY LEFT BLANK

IV. CONCLUSION

In this study, a nanoscale computational technique was developed for atomic or molecular equilibrium under static loads. The technique was based on interactive force equilibrium among atoms using potential function of Classical MD. The interaction among atoms was described by nonlinear springs among them with internal forces. The nanoscale atomic model was also coupled with the finite element method so that boundary conditions could be applied more readily to the model. A variety of example problems with nanoscale defects or atomic dislocations were presented to demonstrate the developed computational technique.

Then, some SWNTs were consedered to estimate the effective stiffness of the nanotubes, which varies with the diameter of SWNT. Based on the estimated elastic modulus of SWNT, the developed computational technique was exploited into a multi-scale analysis of a composite structure. From the sample simulation, using carbon nanotubes as fibers has a positive influence on the effective stiffness of the woven fabric composites. Also, those nano-composites will be used in numerous ways in military as well including the aircraft, body armor, infantry transportation vehicles, and bridges etc. due to its advanced properties such as light weight and high strength.

Using the nonlinear spring concept for the interaction among atoms produced quite reasonable results compared to the ones of other researches and experimental data qualitatively. The developed nanoscale computational technique was computationally efficient and would be a useful tool for design and analysis of materials at the atomic or molecular level.

THIS PAGE INTENTIONALLY LEFT BLANK

V. RECOMMENDATIONS

This work developed a simulation technique utilizing the different potential functions. Nonlinear spring concept for interaction among atoms was used to predict the atomic behavior in nanoscale, the effective stiffness of single wall nanotube, and composites made of carbon nanotubes. There could be various and numerous applications to this developed computational technique. It is recommended that further study be conducted in the following areas:

- Another computational technique is recommended to model and simulate atomistic behavior of materials under dynamic loads such that atomic or molecular behavior could be examined under the various dynamic load cases.

- Other mechanical properties of SWNT can be investigated such as bending stiffness, torsion stiffness or shear modulus of the nanotubes changing the static loads and constraints.

- For more accurate atomic potentials, other potential functions from quantum mechanics like ab initio method could be exploited into our developed computational technique.

- It is recommended that with designed nano-composites, actual models being used in military such as body armor or bridges, which are made of nano-composites can be simulated and tested if it's efficient and applicable or not.

THIS PAGE INTENTIONALLY LEFT BLANK

LIST OF REFERENCES

[1] D. Srivastava, M. Menon, K. Cho, "*Computational Nanotechnology with Carbon Nanotubes and Fullerenes*", Computing in Science & Engineering, 42-48, July/August 2001.

[2] M. Meyyanppan, D. Srivastava,"*Carbon Nanotubes: A Revolution in Nanotechnology*", IEEE Potentials, Vol. 19 (3), pp. 16-18, August/Sepember. 2000."

[3] Q.Qian, E.C. Dickey, R. Andrews, T. Rantell, Applied Physics Letter, 76, 2868,2000

[4] D. Srivastava, C. Wei, K. Cho, "*Computational Nanomechanics of Carbon Nanotubes and Composites*", Applied Mechanics Review,

[5] D. Srivastava, S. Barnard, in Proceedings of IEEE Supercomputing '97(SC '97), 1997.

[6] B.I. Yakobson, C.J. Brabec and J. Bernholc, Physics Review Letter, 76, 2511, 1996.

[7] C.Wei, D. Srivastava, K. Cho, "*Molecular Dynamics Simulations of the Temperature Dependent Plastic Collapse of Carbon Nanotube under Axial Compression,*" Comp. Modeling in Engineering and Sciences, submitted, 2001.

[8] J. Tersoff, R.S. Ruoff, "*Structural Properties of a Carbon-Nanotube Crystal*", Physical Review Letters, 73, 676-679, August 1994.

[9] C.F. Cornwell, L.T. Wille "*Elastic Properties of Single-Walled Carbon Nanotubes in Compression*", Solid State Communications, 101, 555-558, 1997.

[10] T. Ozaki, Y. Iwasa, T. Mitani, "*Stiffness of Single-Walled Carbon Nanotubes under Large Strain*", Physical Review Letters, 84. 1712-1715, 2000.

[11] A. Krishnan, E. Dujardin, T.W. Ebbesen, P.N. Yianilos, M.M.J. Treacy, "*Young's Modulus of Single-Walled Nanotubes*", Physical Review B, 58, 14013-14019, November 1998.

[12] J.E. Sinclair, "*The Influence of the Interatomic Force Law and of Kinks on the Propagation of Brittle Crack*", Philosophical Magazine, 31, 647-671, 1975.

[13] S. Kohlhoff, P. Gumbsch, H.F. Fischmeister, "*Crack Propagation in B.C.C. Crystals Studied with a Combined Finite-Element and Atomistic Model*", Philosophical Magazine A, 64, 851-878, 1991.

[14] M.S. Daw, M.I. Baskes, C.L. Bisson, W.G. Wolfer, "*Application of the Embedded Atom Method to Fracture, Dislocation Dynamics, and Hydrogen Embrittlement*", Sandia Report, SAND86-8660, March 1986.

[15] C. Hsieh, R. Thomson, "*Lattice Theory of Fracture and Crack Creep*", Journal of Applied Physics, 44, 2051-2063, 1973.

[16] R.G. Hoagland, M.S. Daw, S.M. Foiles, M.I. Baskes, "*An Atomic Model of Crack Tip Deformation in Aluminium Using an Embedded Atom Potential*", J. Mater. Res., 5, 313-324, 1990.

[17] M. Mullins, "*Computer Simulation of Fracture Using Long Range Pair Potentials*", Acta Metall., 32, 381-388, 1984.

[18] J.M. Haile, "*Molecular Dynamics Simulation: Elementary Method*", John Wiley & Sons, New York, 1997.

[19] D. C. Rapaport, "*The Art of Molecular Dynamics Simulation*", Cambridge University Press, Cambridge, United Kingdom, 1995.

[20] L. A. Girifalco and V. G. Weizer, "*Application of the Morse Potential Function to Cubic Metals*", Physical Review, 114 (3), 687-690, 1959.

[21] D.W. Brenner, "*Empirical Potential for Hydrocarbons for Use in Simulating the Chemical Vapor Deposition of Diamond Films*", Physical Review B, 42 (15), 9458-9471, November 1990.

[22] Y.W. Kwon and L.E. Craugh, "*Progressive Failure Modeling in Notched Cross-Ply Fibrous Composites*", Applied Composite Materials, 9(1), 63-74, January 2001.

[23] Y.W. Kwon and A. Altekin, "*Multi-level, Micro-Macro Approach for Analysis of Woven Fabric Composites*", Journal of Composite Materials, in print.

INITIAL DISTRIBUTION LIST

1. Defense Technical Information Center
   Ft. Belvoir, Virginia

2. Dudley Knox Library
   Naval Postgraduate School
   Monterey, California

3. Professor Young W. Kwon
   Department of Mechanical Engineering
   Naval postgraduate school
   Monterey, CA

4. Department Chairman
   Department of Mechanical Engineering
   Naval Postgraduate school
   Monterey, CA

5. Engineering & Technology Curricular Office (Code34)
   Naval Postgraduate school
   Monterey, CA

6. Dr. Chanman Park
   Naval Postgraduate school
   Monterey, CA

7. Captain Sunghoon Jung, ROK Army
   404-12 Sujeongdong,
   Yosu, Jeonnam, Republic of Korea